THE UNIVERSITY OF OKLAHOMA

GRADUATE COLLEGE

STRUCTURAL CHARGE SITE INFLUENCE ON THE INTERLAYER PROPERTIES OF EXPANDABLE THREE-LAYER CLAY MINERALS

A DISSERTATION

SUBMITTED TO THE GRADUATE FACULTY

in partial fulfillment of the requirements for the degree of

DOCTOR OF PHILOSOPHY

BY

RAYMOND L. KERNS, JR.

Norman, Oklahoma

1966

STRUCTURAL CHARGE SITE INFLUENCE ON THE INTERLAYER PROPERTIES OF EXPANDABLE THREE-LAYER CLAY MINERALS

APPROVED BY

Charles J. Mankin

[illegible]

Edward C. Jonas

David B. Kitts

George T. Stone

DISSERTATION COMMITTEE

ACKNOWLEDGMENTS

Sincerest thanks to Dr. Charles J. Mankin for his advice and direction during the course of the investigation. His influence as an educator, scientist, and friend are highly valued by the writer.

Conversations and correspondence with Dr. Edward C. Jonas from the University of Texas were instrumental in providing the inspiration and enthusiasm for initiating this investigation. He also read and offered suggestions toward the improvement of the manuscript.

Dr. George T. Stone and Dr. David B. Kitts read the manuscript. Their advice and criticisms were gratefully received.

Fellow students and colleagues who suffered through various stages of the research and who contributed to the final completion of the study were: William H. Bellis, Frederick H. Manley, Jr., Clayton Nichols, Dah Chen Wu, and Her Yue Wong. To these fellows, grateful thanks.

Appreciation is extended to the Continental Oil Company which provided support for one academic year by means of a greduate fellowship.

To Gloria, sincerest appreciation for all the sacrifices required of a student's wife and for active participation in reading, editing, and typing the manuscript in its preliminary and final forms.

TABLE OF CONTENTS

LIST OF TABLES

LIST OF ILLUSTRATIONS

Figure Page

STRUCTURAL CHARGE SITE INFLUENCE ON THE INTERLAYER PROPERTIES OF EXPANDABLE THREE-LAYER CLAY MINERALS

INTRODUCTION

The most distinctive property of montmorillonites and vermiculites is their ability to absorb and retain water between individual three-layer units at low temperatures over a wide range of relative humidities. This phenomenon is directly responsible for the somewhat variable c-axis dimensions of these minerals (particularly montmorillonite) and may be observed through x-ray diffraction measurements of the d-spacings of the (001) planes.

Studies of this property made by Nagelschmidt (1936) and Hofmann and Bilke (1936) indicated a continuous variation of the (001) d-spacing with the total number of water molecules present. Bradley, Grim, and Clark (1937) provided evidence that the water molecules in a hydrogen-montmorillonite were absorbed in a step-wise fashion as water molecule layers. Later works have confirmed the concept of water uptake as a step-wise addition of mono-molecular layers. Mooney, Keenan, and Wood (1952) provided information on the step-wise hydration of montmorillonites as a function of the interlayer cation chemistry and relative humidity.

Many of the earlier studies were concerned with the organization and arrangement of the water molecules in the interlayer region. Bradley, Grim, and Clark (1937) considered the water molecules as close-packed layers. Hendricks and Jefferson (1938) favored the arrangement of oxygen ions in the tetrahedral layer and the interaction of interlayer water with the crystal lattice as the controlling factors. On this basis they proposed a hexagonal array of the water molecules in the interlayer region. Mering (1946), however, considered the interaction of the water molecules with the interlayer cations. He described the two-layer state of hydration as complexes of calcium ions surrounded by six water molecules. These are oriented so that the Ca-H_2O octahedra are resting on (111) faces against the tetrahedral sheets. This state results in a (001) d-spacing of 14.0 Å. At higher relative humidities a true two-layer water molecule arrangement results in an expansion of the (001) plane to about 15.4 Å.

Other investigations have utilized heating techniques in conjunction with x-ray diffractometry to obtain data on the hydration or dehydration states of expandable mica-type minerals. Rowland, Weiss, and Bradley (1956) used oscillating diffractometer furnace techniques to show the differences in the stability of hydrated montmorillonites as a function of the temperature and type of interlayer cation. They indicated, for Ca-, Mg-, Mn-, Li-, and H-montmorillonites and vermiculites, that an octahedrally-coordinated relationship exists

between the interlayer cations and the absorbed water molecules. The montmorillonites were shown to pass from 14.5 Å (octahedral) to 11.5 Å (one water-layer) states as they were heated to higher temperatures. Montmorillonites with Na and K as the interlayer cations also revealed a single water-layer state, but the d-spacing at 12.4 Å for these materials suggested that the water-cation arrangment is not exactly the same as the partially dehydrated crystallite having smaller monovalent and divalent cations. Considering the temperature at which final collapse of the (001) d-spacing occurs as a measure of the cation to water molecule bond strength, the order from stronger to weaker bonding energies is Mg > Ca > Li > Na > K. This is, in part, supported by the DTA data of cation exchanged vermiculite provided by Barshad (1948). Similar data for exchanged montmorillonite and vermiculite are presented in this study.

The dehydration mechanism of vermiculites has been studied and described by Walker (1956). The progressive collapse from a 14.81 Å phase through 14.36 Å, 11.59 Å, 10.6 Å mixed-layer phases to a final 9.02 Å totally collapsed state was discussed in detail. The more important aspects of the study described the location of the Mg ions at the center of water molecule octahedra in the 14 Å states. As the interlayer octahedra are disrupted at higher temperatures with loss of water molecules, magnesium ions migrate to positions adjacent to the tetrahedral layers directly over the Si and Al sites. The 11.59 Å phase consists of Mg ions located at

these positions in imperfect octahedral coordination with respect to three oxygen ions of the tetrahedral layer and three water molecules. The water molecules are adjacent to the opposing tetrahedral layer and occur as incomplete single monomolecular layers interleaved with three-layer structural units.

On the basis of hydration and dehydration studies, evidence is strongly in support of definite cation-water molecule interactions in the interlayer region. The general consensus is, at least at low to intermediate states of hydration, that the interlayer region of expandable clays is occupied by water-cation complexes rather than simple monomolecular water layers. The initial state of hydration involves the separation of the three-layer units and development of a hydrated complex with the interlayer cations. The initial hydration energy, which is a function of the ionic potential of the cation and the partial pressure of water vapor in the system, must be sufficiently large to overcome the strength of the crystal lattice to interlayer cation bond. A factor contributing to the expandability of three-layer clay minerals is the small magnitude of the forces with which successive lattice units are held together. A property that contributes to the total force of resistance to expansion is the surface charge density. This is an expression of the number of equivalent lattice to interlayer cation bonds per unit area or commonly expressed as equivalents per unit cell.

The expected association would be that clay minerals having large surface charge densities are not likely to undergo expansion, whereas clay minerals with low surface charge densities will exhibit more intense properties of interlayer water absorption.

A detailed study by Hofmann, et al. (1956) showed a correlation between the intensity of interlayer swelling properties and the surface charge densities of a selected suite of three-layer clay minerals. Hofmann's data indicated that less than 0.55 equivalents of charge per unit cell results in a crystal lattice that is readily susceptible to interlayer water absorption. Clay minerals with lattice charge deficiencies in excess of 0.65 equivalents per unit cell, when saturated with potassium, have a 10.3 Å basal spacing under both wet and dry conditions.

Another factor which has been considered, but not demonstrated, is the contribution of the site of the lattice charge deficiencies to the swelling properties of montmorillonites and vermiculites. Marshall (1936) and MacKenzie (1950) have suggested that the strength of the bond between the cation and the lattice may be a considerable factor in determining the extent and ease with which water absorption takes place. If the bonding energies are considered ideally electrostatic, then the force resisting separation of adjacent

three-layer units may be expressed as Coulomb's law:

$$F \propto \frac{C^+ C^-}{r^2} \qquad 1$$

where C^+ and C^- represent the charges (or valences) entering into the bond formation and r is their distance of separation. This would indicate that the distance of separation of a given interlayer cation from an equivalent charge deficiency is a critical factor in determining the magnitude of the bond strength involved. This would necessarily imply then, that a charge deficiency originating in the tetrahedral layer would result in a stronger lattice-cation bond than a similar situation where the unsatisfied lattice charge is located in the octahedral layer. The expected result of such differences, if significant, should then be reflected as a difference in the swelling behavior of mica-type materials having predominantly tetrahedral versus octahedral layer charge deficiencies.

NATURE OF THE INVESTIGATION

An unfortunate aspect of Hofmann's (1956) data is, that within the suite of samples included in his study, there is a direct relationship between minerals of low charge density and those possessing predominantly octahedral charge deficiency sites. The samples that Hofmann chose to represent three-layer clay minerals of high surface charge density had predominantly tetrahedral charge deficiencies. It is impossible, therefore, to separate the independent influence (if any) of surface charge density and lattice charge site locations on the expanding properties of the three-layer clay minerals included in his study.

The purpose of this study was to investigate the contribution of lattice charge sites to the swelling properties of expandable three-layer clay minerals. The first requirement involved the selection of samples that were significantly different in the tetrahedral and octahedral contributions to the total surface charge density. The selection was made on the basis of detailed chemical and structural analyses so that an absolute correlation between high surface charge density and predominantly tetrahedral charge deficiencies was

not possible. Any differences in the swelling behavior of the various materials could then, hopefully, be correlated to total surface charge density or structural charge site. The effect of difference in the interlayer cation composition had to be eliminated. This was accomplished by saturating portions of each sample with the same cation. These samples were then subjected to various reproducible conditions of relative humidity and the interlayer water absorption of samples containing identical interlayer cations were directly compared by x-ray diffractometry measurement of the (001) d-spacings. Under these conditions differences in the swelling behavior of identically cation-saturated minerals could be attributed to properties of the mineral lattice itself.

STRUCTURE OF THREE-LAYER CLAY MINERALS

The Mica Model

The model for the three-layer clay minerals has evolved from the pioneering work of Pauling (1930) and Bragg (1937). Many studies have been conducted which have resulted in refinements of the basic mica structure, but the fundamental framework has undergone no significant modification. A brief description of the lattice is presented to provide a basis for the ensuing discussion.

Tetravalent silicon cations and trivalent aluminum cations in four-fold coordination with oxygen anions form a continuous two dimensional array. These tetrahedra share three oxygen ions with nearest neighbors creating an approximate hexagonal pattern. The unshared apical oxygens are all considered to be pointing in the same direction. Two such sheets are then considered to be arranged in such a manner that the apical oxygens interpenetrate a common region between the sheets. Divalent or trivalent cations, most commonly aluminum, magnesium, and iron, occupy octahedral coordination sites with respect to the apical oxygens of both sheets. The vacant anion sites in the octahedra are filled with hydroxyl

and, rarely, fluorine anions. Charge deficiencies due to isomorphous substitutions within the lattice are balanced by interlayer monovalent and divalent cations such as potassium, sodium, calcium, or magnesium. These interlayer cations occupy positions between individual three-layer packets and are considered to be present in close proximity to the hexagonal holes of the tetrahedral layers. Large cations, such as potassium, are considered to have twelve-fold coordination with respect to the more or less hexagonally arranged oxygen ions of adjacent tetrahedral layers.

The total number of negative charges per unit-cell is fourty-four. These are attributed to twenty oxygen ions and four hydroxyl ions in the unit-cell formula. The conventional notation for structural formulae is based on the half unit-cell. This allows for twenty-two negative charges attributed to ten oxygen ions and two hydroxyl ions.

The ideal pyrophyllite structure may be written:

$$Al_2Si_4O_{10}(OH)_2$$

where the six negative octahedral charges are balanced by six positive charges of the two trivalent aluminum ions. The tetrahedral layer negative charges are satisfied by the tetravalent silicon ions. There is no net charge on the lattice and individual three-layer units are held together by residual forces on the interlayer surfaces, probably on the order of van der Waals bond strengths. Similarly, an ideal struc-

ture may be written for talc:

$$Mg_3Si_4O_{10}(OH)_2$$

wherein the lattice charges are similarly balanced.

The two extremes of ideal structures are those in which trivalent ions fill two-thirds of the available octahedral layer positions or divalent ions fill all available octahedral sites. This has resulted in the terms dioctahedral and trioctahedral for the layer-lattice silicates.

A typical example of a dioctahedral mica is muscovite, for which the ideal formula is:

$$KAl_2(Si_3Al)O_{10}(OH)_2$$

Interlayer monovalent potassium ions neutralize the net negative charge deficiency caused by the sugstitution of a trivalent aluminum cation for a tetravalent silicon cation in the tetrahedral layer. Similarly, the ideal structural formulae of two trioctahedral micas are shown by biotite:

$$K(MgFe^{+2})_3(Si_3Al)O_{10}(OH)_2$$

and phlogopite:

$$KMg_3(Si_3Al)O_{10}(OH)_2$$

in which interlayer potassium balances tetrahedral charge deficiencies.

Montmorillonites

The term, montmorillonite, has three connotations in clay meneralogy (MacEwan, 1961). In the first sense it is used to distinguish the whole group of three-layer clay minerals which

have similar properties, particularly in their ability to reversibly release and absorb interlayer water at low temperatures. In the second sense the term refers to a sub-group of clay minerals of this same major group where individual members are chemically composed of silicon, aluminum, and magnesium. Another use of the term montmorillonite is for a specific mineral of approximately the same composition as the type mineral described by Damour and Salvetat (1847). MacEwan (1961), and others of the (British) Clay Minerals Group would prefer to substitute the term smectite as a major group name. However, this term has not been generally accepted in North America.

The most widely accepted structure for the montmorillonite clay minerals is one that was initially proposed by Hofmann, Endell, and Wilm (1933), subsequently modified by Marshall (1935), Maegdefrau and Hofmann (1937), and later by Hendricks (1942). This structure is primarily based on the pyrophyllite (and talc) model, and individual members of the group are named on the basis of gross chemical differences due to compositional variations in the octahedral layer and the amount of aluminum for silicon substitution in the tetrahedral layer.

In the dioctahedral members, an ion for ion substitution of a divalent ion, such as magnesium, for a trivalent ion, such as aluminum, results in a charge deficiency which may be balanced by cations in the interlayer and edge positions.

Many montmorillonites also have a lattice charge deficiency due to tetrahedral layer substitutions of aluminum for silicon. The ratio of Al/Si in the tetrahedral layer is commonly much lower in montmorillonite minerals than has been observed in the more coarsely crystalline mica counterparts. Trioctahedral montmorillonites of an approximate talc composition, but possessing interlayer cations and swelling properties, are called saponites. Other clay mineral names for members of the montmorillonite group arising from variations in the composition of the octahedral layer are nontronite (iron), sauconite (zinc), and volkhonskoite (chromium). Table 1 lists some of the ideal structural formulae for members of the montmorillonite group as presented by MacEwan (1961).

Evidence is overwhelming in support of distinct dioctahedral and trioctahedral montmorillonite structures. Ross and Hendricks (1945), published numerous structural formulae calculated from chemical analyses and reported a range of octahedral layer populations between 2.00 to 2.22 and 2.88 to 3.00 (per half unit-cell). Any intermediate structures at this time are thought to represent mixtures of discrete dioctahedral and trioctahedral types.

Further modifications of the montmorillonite model were proposed by Edelman and Favejee (1940). They suggested that in the tetrahedral layer of montmorillonites some of the tetrahedra are inverted and these apical sites are occupied by hydroxyl ions that project into the interlayer region. The

TABLE 1

IDEAL STRUCTURAL FORMULAE FOR SOME MONTMORILLONITE MINERALS*

Dioctahedral Types
Montmorillonite (Si/Al 2:1): $(Al_{1.67}Mg_{0.33})Si_4O_{10}(OH)_2 M^+_{0.33}$
Beidellite (Si/Al 2:1): $Al_2(Si_{3.67}Al_{0.33})O_{10}(OH)_2 M^+_{0.33}$
Nontronite: $Fe_2^{+3}(Si_{3.67}Al_{0.33})O_{10}(OH)_2 M^+_{0.33}$
Trioctahedral Types
Saponite: $Mg_3(Si_{3.67}Al_{0.33})O_{10}(OH)_2 M^+_{0.33}$
Hectorite: $(Mg_{2.67}Li_{0.33})Si_4O_{10}(OH)_2 M^+_{0.33}$
Sauconite (Typical Formula): $(Zn_{2.40}Al_{0.22}Fe^{+2}_{0.17}Mg_{0.18})(Si_{3.47}Al_{0.53})O_{10}(OH)_2 M^+_{0.35}$

*From MacEwan (1961). The symbol M indicates interlayer cations which may be monovalent sodium or, less commonly, potassium. Divalent cations such as calcium and magnesium are also common interlayer constituents.

dissociation of these hydroxyls was then postulated to account for the high cation exchange capacity of montmorillonites. This concept has not been widely accepted by workers in clay mineralogy. The standard model at the present time is that most recently defined by Hendricks (1942).

The main property that distinguishes montmorillonites from other three-layer mica type clay minerals is the ability to reversibly absorb interlayer water. This gives rise to the highly variable (00ℓ) d-spacings of these minerals and is referred to as the expandable or swelling property of this group of minerals. This characteristic also applies to the ability of members of this group to absorb onto the interlayer surface certain polar organic molecules such as ethylene glycol or glycerol which also affect the (00ℓ) d-spacings.

Vermiculite

The term vermiculite is used as a mineral name for clay size particles as well as macroscopic crystals of approximately the same structure and chemical composition. More studies have been conducted on the properties of large crystals of vermiculite than have been attempted on clay-size materials. An ideal structural formula for vermiculite as written by Walker (1961) is:

$$Mg_3(Si,Al)_4O_{10}(OH)_2Mg_{0.35}{}^{4.5H_2O}$$

where three magnesium ions fill the half unit-cell octahedral positions. The Al/Si ratio is commonly 1/2 to 1/3. The

interlayer region is occupied by cations, commonly magnesium, which balance the negative lattice charge deficiencies. Water molecules absorbed between the layers average about 4.5 molecules per half unit-cell at normal humidities with Mg as the interlayer cation.

Investigations using two-dimensional Fourier syntheses have shown that the water molecules are arranged on a two-layer basis and are octahedrally coordinated around the interlayer magnesium ions which occur midway between the three-layer structural units (Mathieson and Walker, 1954). The interlayer water may be driven off reversibly at low temperatures. Large crystals that are heated rapidly to high temperatures release the interlayer water with such force that the individual booklets exfoliate and expand to many times their original volume.

The basic model for vermiculite is the talc structure. A substitution of aluminum for silicon in the tetrahedral layer creates a charge deficiency which is satisfied by inter-layer cations. Vermiculite is similar to the mica member, phlogopite. The difference is mainly in the interlayer cation chemistry and the expandable nature of vermiculite. Some clay minerals of vermiculite composition are probably included with the saponite minerals in the montmorillonite group. Walker (1961) refers to differences in clay-size vermiculite and saponite as a function of surface charge density. Vermiculites with low layer-charge have swelling properties more consistent with the minerals of the montmorillonite group. Hofmann, et al.

(1956), have provided evidence suggesting a continuous gradation between saponite and vermiculite. The main criterion for distinguishing the two is based on their relative swelling properties, the expandable nature of montmorillonite subjected to treatment with polar organic compounds such as ethylene glycol, and the non-expandable nature of true vermiculites exposed to a similar treatment.

A wide range of isomorphous substitution of divalent and trivalent ions for octahedral magnesium has been observed. Separate mineral terms have not been generally accepted for members of the vermiculite group with various compositions as with the minerals of the montmorillonite group. One exception may be the iron-free vermiculite described by Weiss and Hofmann (1951), called batavite.

EQUIPMENT

X-ray Diffraction and Fluorescence

X-ray diffraction data were obtained with North American Phillips (Norelco) and Siemens x-ray diffraction equipment. These units are equipped with copper target tubes which provide the x-ray sources. The cameras are motor-driven diffractometers in which flat specimens can be mounted tangent to the focusing circle. A range of slit aperture systems and goniometer scanning rates was employed. Scintillation counters were used as detectors. The spectrum of copper radiation was passed through nickel filters to enhance the copper K-α line with respect to K-β. Additional filtering was accomplished by manipulation of the baseline and window settings in the pulse-height analyzing circuits. Data were recorded in the form of diffractograms on motor driven fixed-speed strip charts.

Chemical analyses were obtained with a Siemens vacuum x-ray spectrometer. Primary excitation radiation was supplied by a high intensity chromium target tube. Analyzing crystals are lithium fluoride and gypsum. A flow-proportional counter was used as a detector and P-10 (ninety percent argon and ten

percent methane) with a 0.06 cubic feet per hour flow rate was used as the detector gas.

Pulse amplitude discrimination was facilitated by a Siemens pulse spectroscope. Spectrograms were recorded on a motor-driven strip chart and intensities of K-α spectral lines for quantitative chemical analyses were recorded with an automatic print-out device. Brickettes of samples for x-ray fluorescence analyses were prepared with a $1\frac{1}{4}$ inch diameter Buehler die and a Paul Weber press.

Differential Thermal Analysis

Differential thermal analyses were run on a Robert L. Stone dynamic gas DTA (Model 13M). Both inconel and stainless steel sample holders were used. Thermocouples are made of a platinum-rhodium alloy, and α-alumina was used as an inert standard. Nitrogen was used as the purging gas in all analyses.

Cation Exchange Capacity

Determinations of cation exchange capacity required the use of an Eberback shaker and several magnetic stirring plates. Titrations with 0.4N sodium hydroxide were made with five-milliliter microburets graduated for direct reading to 0.01 ml (estimates to 0.001 ml). A Beckman Instruments pH meter (Model N) was used for pH measurements.

Particle Size Fractionation

The disaggregation and dispersion of all samples was accomplished with a Powertron Ultrasonics autosonic (Model PA-3001) generator and transducer system. Plum bentonite samples were also dispersed in a Waring blendor. Particle size fractionation to one micron equivalent spherical diameter (ESD) was carried out with standard laboratory glassware and plastic containers of various sizes. Separation of particles of less than one micron was accomplished with a Lourdes Instrument Corporation continuous-flow high-speed centrifuge (Model LCA-1). Distilled water was used as the dispersant in all beneficiation operations.

Particle size reduction by grinding was accomplished with porcelain and agate mortars and pestles. Particle size control in these cases was obtained by hand sieving. A Pitchford Manufacturing Corporation selective uniform particle size grinder (Model 3900) was used to prepare a four-hundred mesh powdered sample of large vermiculite crystals.

Other Equipment

Accurate sample weights, when necessary, were obtained with an analytical balance with an accuracy of 0.0001 gram. Arithmetical calculations were performed on a Friden calculator (Model SRW). Drying of samples and weight loss determinations were accomplished through the use of a low temperature oven set at 60° C and a high temperature furnace operable to 1000° C.

TECHNIQUES

Particle Size Fractionation

Bulk samples of the Plum bentonite from the Bob Mattingly Ranch, Fayette County, Texas, and vermiculite regolith from the Carl Moss Ranch, Llano, Texas, were disaggregated in distilled water with an autosonic generator. The bentonite was also treated somewhat more vigorously by Waring blendor treatments. Particle size separations were obtained by utilizing differential settling velocities according to Stoke's Law. No consideration was given to deviations from spherical shapes of the platy mica and clay particles. The size ranges as reported are meant to be interpreted as equivalent spherical diameter and are indicated as such by the abbreviation ESD.

Particle size fractions to a one micron lower limit were obtained by the standard siphon method (variations of the decantation method). The Plum bentonite particle size fractions 4-6, 2-4, and 1-2 microns (ESD) and the vermiculite particle size fractions 16-32, 8-16, 4-8, 2-4, and 1-2 microns (ESD) were obtained in this manner. Plum bentonite fractions of 1/2-1, 1/10-1/2, and 5/100-1/10 micron (ESD) and vermiculite fractions of 1/2-1, 1/4-1/2, 1/10-1/4, and

5/100-1/10 micron (ESD) were separated by means of high speed continuous flow centrifuge methods.

The size-fractioned materials were dried in an oven preset at 60° C and were then ground to powders with a mortar and pestle. In order to avoid any adverse affects due to grinding, a short period of grinding was followed by hand sieving through an eighty-mesh screen. The eighty-mesh powdered aggregates were then homogenized by the shaking mechanism of the Pitchford grinder and stored in glass vials.

Samples of the large yellowish-brown crystals of Llano vermiculite were reduced to a suitable particle size for x-ray powder diffraction, x-ray fluorescence, and differential thermal analysis. Large booklets of this material were chopped to about five millimeters in size and further reduced to four-hundred mesh in the Pitchford uniform particle size grinder. This powdered material was also homogenized by vigorous shaking.

X-ray Diffractometry

Random orientations were prepared by sieving the powdered samples directly onto glass slides coated with a thin veneer of petroleum jelly. After allowing a few minutes for sufficient adhesion, the slide was inverted and the excess powder removed by tapping lightly on the side of the mount. The (00ℓ) oriented samples were prepared by dispersing a small amount of material in distilled water and placing this on a glass slide

in an oven set at 60° C. After drying, the slide mount was removed and placed in a humidifier. Powders and sedimented slide preparations intended for x-ray diffractometry were humidified for a minimum of eight hours at approximately fifty percent relative humidity before analysis.

Treatments with ethylene glycol to investigate the expandability of the material were carried out on (00ℓ) oriented samples. These were placed in a vacuum grease-sealed aluminum "dessicator" containing ethylene glycol. The system was maintained at 60° C for a minimum of eight hours so that the slides were in an atmosphere saturated with ethylene glycol vapor for a prolonged period. The samples were analyzed by x-ray diffraction immediately upon removal from the glycol environment.

All diffractograms were obtained with goniometer scanning speeds of one degree two-theta per minute. The system for the Norelco unit was one degree for the collimating and receiving slits and a 0.006 inch scatter slit was used. The Siemens diffractometer was operated with a one millimeter collimating slit and a two-tenths millimeter receiving slit. A variable knife edge on the sample holder acted as a scatter slit. Chart speeds were set at one-half inch per minute on the Norelco unit and one centimeter per minute on the Siemens recorder. Scale factor settings were made to maintain all peaks on scale. Lower scale factors were used for some analyses to enhance weaker diffraction lines. Diffraction scans

from two to sixty-five degrees two-theta were made for all samples. All powder diffraction scans and (00ℓ) oriented diffraction scans on the better crystalline samples were run to ninety degrees two-theta. The copper target x-ray tubes were operated at thirty-five kilovolts and eighteen milliamps. The copper spectrum was filtered with nickel foil and proper baseline and window settings in the pulse height analyzing circuit were made to permit near monochromatic selection of the copper K-α wavelength.

Differential Thermal Analysis

All powders were humidified for at least eight hours before they were placed in the DTA sample holder. Care was taken to make all runs as consistently uniform as possible. The time lapse from removal from the humidifier to the beginning of each run was held to a minimum, which was always less than five minutes. The amount of sample placed in the sample holder and the degree of packing were the most difficult variables to control. Nitrogen was used as a purging gas in every run and the manometer mercury level was maintained at the 2.0 mark (relative scale). The microvolt setting was kept at eighty and the calibration factor of 1.0 was checked before each run. Furnace heating rates were programmed for 10° C per minute. All runs were made from room temperature to 1020° C with the stainless steel sample holder and to 1080° C with the inconel sample holder.

Cation Exchange Capacity

Cation exchange capacities (CEC) were determined in triplicate and reported as milliequivalents of NaOH per one hundred grams of sample on an oven-dry basis (dried at 170° C). The technique used is referred to as "the continuous-titration sodium hydroxide technique". The method involves the accurate weight determination of a sample weighing approximately one gram. The sample is then dispersed in distilled water and converted to the hydrogen form with Dowex 50W-X4 resin in the H^+ form. The suspension is separated from the resin by wet sieving and the total volume brought to five hundred milliliters by adding distilled water. The initial pH was measured and a small amount (about 0.10 milliliter) of 0.4000N sodium hydroxide added from a microburet. After twenty minutes of mechanical mixing on a magnetic stirring plate, the pH was measured and recorded. This titration process was repeated until a pH of 10.0 or higher was obtained. The data were then plotted as pH versus meq per 100 grams of oven-dry sample. The cation exchange capacity (CEC) for the sample was taken as the average value of the three curves interpolated at a pH of 7.0.

Chemical Analyses

Weight losses measured at 170° C were taken as H_2O^-. This value was subtracted from the total weight loss on firing at 1000° C to determine H_2O^+. Quantitative chemical analyses

for SiO_2, Al_2O_3, Fe_2O_3, MgO, CaO, K_2O, and TiO_2 were obtained by x-ray fluorescence methods.

All samples were prepared for x-ray fluorescence analyses by accurately weighing and mixing air-dry samples with ten percent (by weight) polyvinyl alcohol (PVA) as a binding agent. These were thoroughly homogenized by shaking and pressed into brickette form in a $1\frac{1}{4}$ inch Buehler die at fifteen tons total load on a Paul Weber press. Suitable oxide standards were prepared in the same way.

The intensity of the first order K-α line was used to determine the percentage of each element. Two-minute counts were taken by a step-scanning process and intensities were reported in counts per minute. The percentage by weight of the oxides of each element was interpolated from a standard curve for each element. This curve was constructed from x-ray fluorescence analyses of standard samples of silicate composition for which accurate chemical analyses were available from independent sources. The data for the standard curves were obtained during the time that the chemical analyses were being run.

MONTMORILLONITE

Plum Bentonite

The montmorillonite selected for this study was extracted from a bulk sample of the Plum bentonite. This unit occurs stratigraphically at the base of the Manning formation of the Jackson group (Eocene) in the Texas Gulf Coast sequence. The particular sample involved in this study came from a pit on the Bob Mattingly Ranch, Fayette County, Texas. The locality is described by Folk, Hayes, and Brown (1961) as one of the best outcrops of the Plum bentonite. About twelve feet of white, hard, conchoidally fracturing, and massively bedded bentonite is exposed at this site.

The Plum bentonite is one of several Upper Eocene and Oligocene bentonite and volcanic ash beds which crop out in the Texas Gulf Coast area. Persons interested in the stratigraphy of this region are referred to the publication of Sellards, Adkins, and Plummer (1932). The petrology of the Tertiary bentonites of Texas was studied by Roberson (1964). The study involved a petrographic and x-ray diffraction investigation of the mineralogical content of these bedded deposits. The dominant mineral present is a 15 Å montmoril-

lonite with minor amounts of illite and kaolinite observed in some samples. Non-clay mineral phases observed to be present are quartz, cristobalite, feldspar, mica, and calcite. Samples from the lower Manning formation (Plum bentonite section) contain a well-crystallized 15 Å montmorillonite as the only clay mineral present. These samples also contain a sizeable amount of cristobalite (10 to 20 percent), but no other non-clay mineral phases were detected.

X-ray Diffraction Data

X-ray analyses indicate the presence of two mineral phases in the Plum bentonite sample. The dominant constituent is a dioctahedral montmorillonite that has an intense (001) diffraction peak at 5.90 degrees two-theta, a moderate (02*l*), (11*l*) edge reflection at 62.20 degrees two-theta. The less abundant constituent has only a broad peak at 21.70 degrees two-theta, and indicates the presence of alpha-cristobalite.

Figure 1 contains the diffractometer traces from two to forty-eight degrees two-theta of bulk, 4-6, and 5/100-1/10 micron samples. Diffractometer traces of the (00*l*) oriented and the ethylene glycol expanded sample of the 5/100-1/10 micron fraction are also illustrated. These data indicate that the cristobalite is concentrated in the coarser fraction (4-6 microns) and is less abundant in the finer fractions (less than one micron). Figure 2 graphically shows the relative

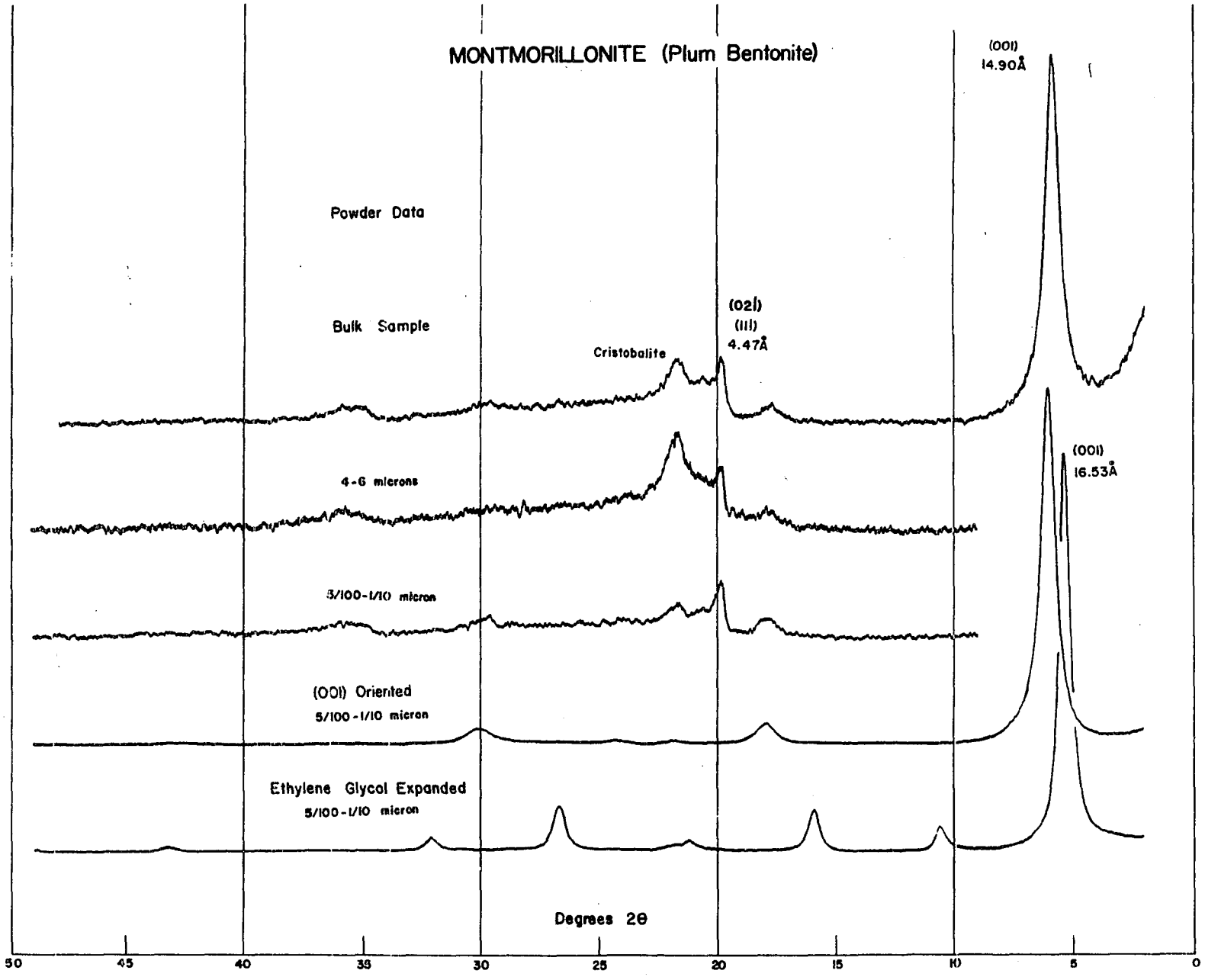

Figure 1. X-ray diffractometer scans of selected Plum bentonite montmorillonite samples.

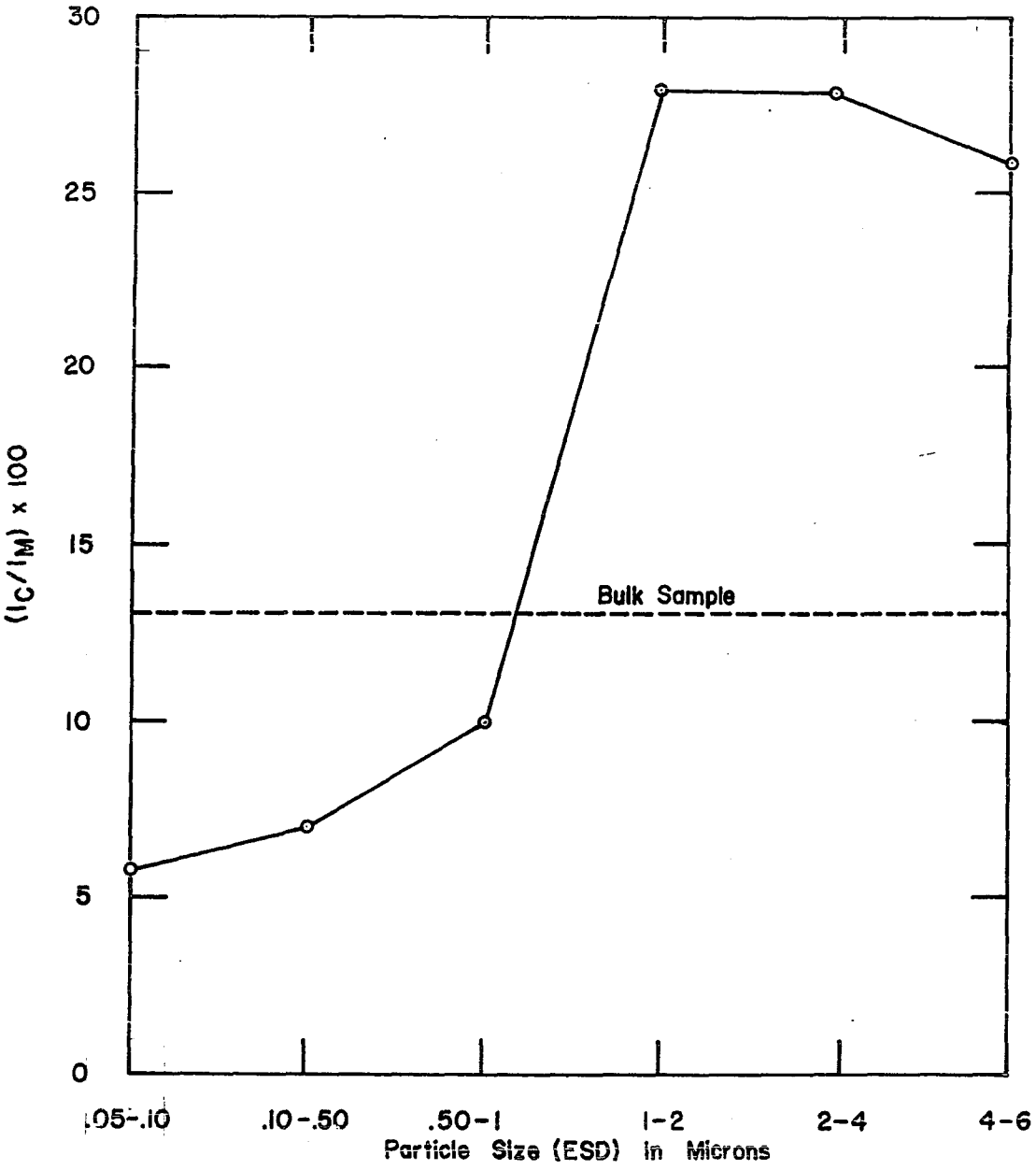

Figure 2. Relative intensity of (101) peak of alpha-cristobalite (I_C) with respect to (001) peak of montmorillonite (I_M). Data are for the size-fractioned Plum bentonite and are based on peak-height measurements of powder diffractograms.

intensity (peak height) of the cristobalite peak with respect to the montmorillonite (001) peak for the various samples.

X-ray diffractometry of the (00ℓ) oriented slide shows four orders of the (001) spacing. The diffraction pattern of ethylene glycol expanded material provides seven observable orders of the (001) peak. The d-spacings and relative intensities of the x-ray diffraction lines of the 5/100-1/10 micron fraction are summarized in Table 2.

TABLE 2

X-RAY DATA: PLUM BENTONITE MONTMORILLONITE (5/100-1/10 micron)*

Miller Indices	Random Orientation		(00ℓ) Oriented		Solvated (00ℓ) Oriented	
	d(Å)	I/I_ox100	d(Å)	I/I_ox100	d(Å)	I/I_ox100
001	14.99	100	14.86	100	16.52	100
002	-	-	-	-	8.34	6
003	4.95	5	4.95	5	5.57	11
02ℓ 11ℓ	4.48	16	-	-	-	-
004	-	-	3.66	1	4.41	2
005	3.02	4	2.97	4	3.34	11
006	-	-	-	-	2.789	4
007	-	-	-	-	-	-
008	-	-	-	-	2.094	1
060	1.495	2	-	-	-	-

*Relative intensities are on the basis of peak height.

The b-axis parameter calculated from the (060) d-spacing of 1.495 Å is 8.870 Å. This positively identifies this montmorillonite as a dioctahedral type.

Differential Thermal Analysis

Humidified powders of all size fractions were subjected to differential thermal analysis. All samples were heated to 1080° C in an inconel sample holder. Figure 3 shows the DTA curves for the bulk, 4-6, and 5/100-1/10 micron samples. They are essentially the same. The only significant variations are in the intensity of the reactions and loss of definition at higher temperatures in the coarser fraction. Figure 4 is a plot of the relative intensity of the low temperature endotherm as linear displacement below the base line versus particle size.

The endothermic doublet at 0 to 100° C is due to loss of surface and interlayer water. The endotherm at 680° C represents dehydroxylation of the octahedral layer. The higher temperature endotherm at 910° C may represent final loss of all traces of octahedral (OH^-) water. The high temperature series of exotherms between 1000 and 1080° C represents the formation of new non-clay mineral phases.

Samples of all fractions of the bentonite were heated to 1000° C for twelve hours. After cooling to room temperature x-ray diffractograms were obtained on the powdered materials. Two phases are distinguishable on the diffractometer traces

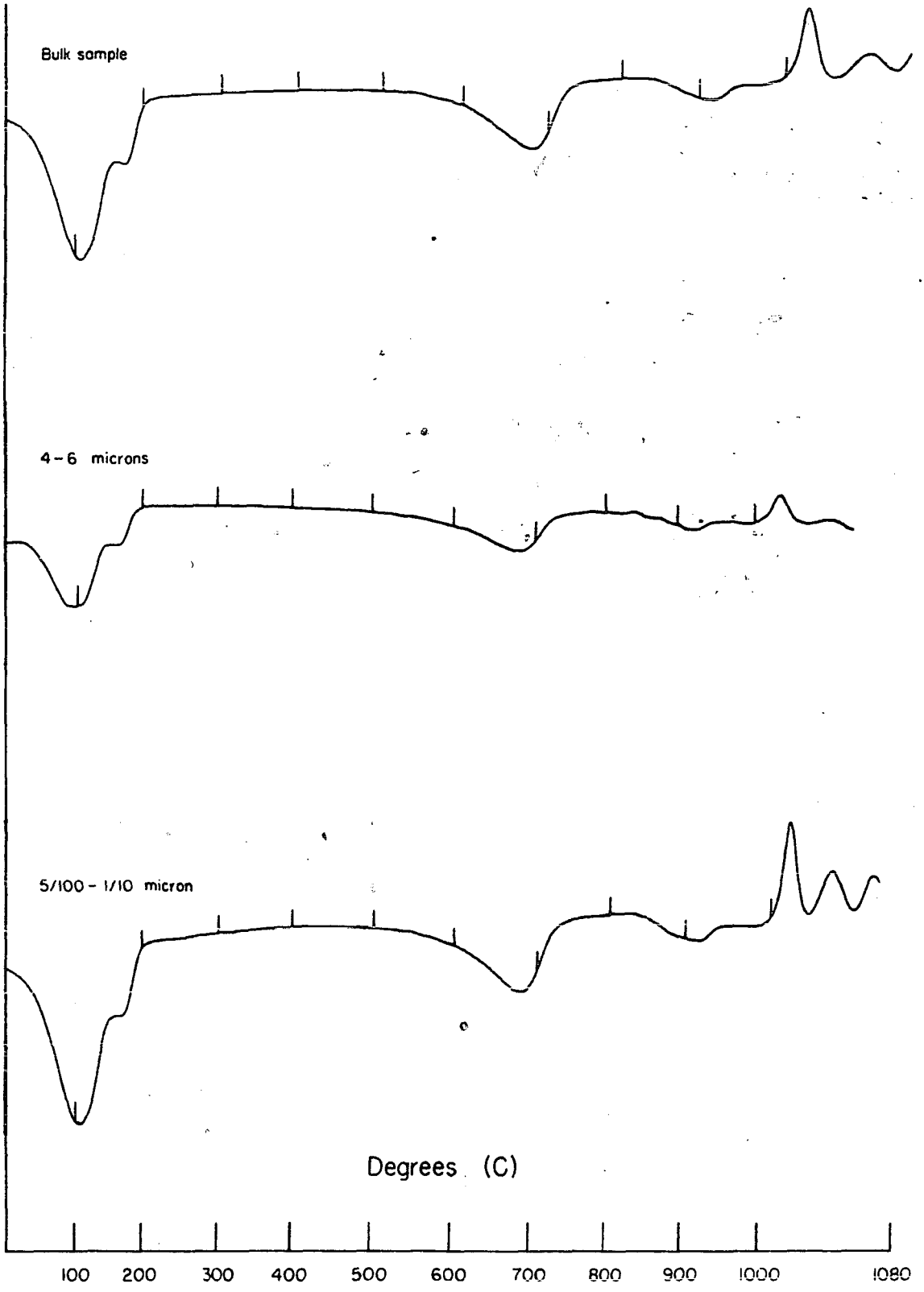

Figure 3. Differential thermal analysis data of Plum bentonite samples.

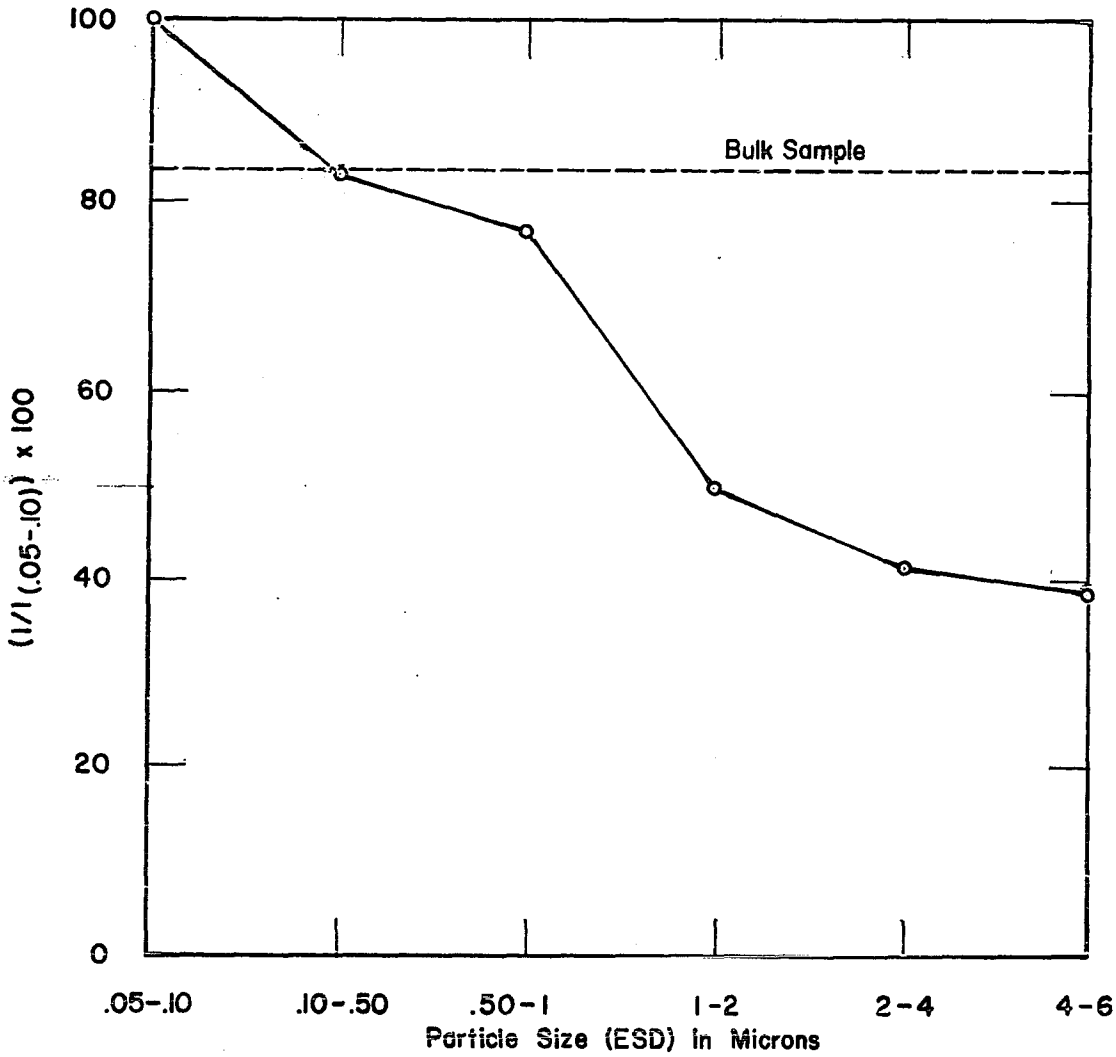

Figure 4. Relative intensity of low temperature de-watering endotherm of size fractions of Plum bentonite montmorillonite with respect to the .05-.10 micron (ESD) fraction. Intensity based on the maximum linear displacement of the endotherm from the baseline as interpreted from the DTA thermograms.

One is alpha-cristobalite and the other is beta-quartz. Figure 5 illustrates the patterns obtained on fired samples of bulk, 4-6, and 5/100-1/10 micron materials. In the coarser fractions alpha-cristobalite is dominant and shows a sharp peak. In the finer fraction beta-quartz is the dominant phase. A small diffraction peak at 27.9 degrees two-theta may indicate the formation of a feldspar, probably anorthite.

Figure 6 illustrates the relative intensities of alpha-cristobalite and beta-quartz in the various size fractions. The particle size is plotted on the abscissa and the factor:

$$\frac{I_c}{I_c + I_Q} \times 100 \qquad 2$$

where I_c represents the intensity of alpha-cristobalite and I_Q represents the intensity of beta-quartz, is plotted on the ordinate.

The formation of a well-crystallized cristobalite phase may be due to the recrystallization of the poorly-ordered cristobalite present in the unfired material. It is definite that the intensity of the alpha-cristobalite peak is directly correlated to the increased particle size, both in the unfired and fired samples. Some of the alpha-cristobalite may also be forming from the montmorillonite lattice. However, it seems that the predominant high temperature phase formed from the clay material at 1000° C is beta-quartz. The intensity

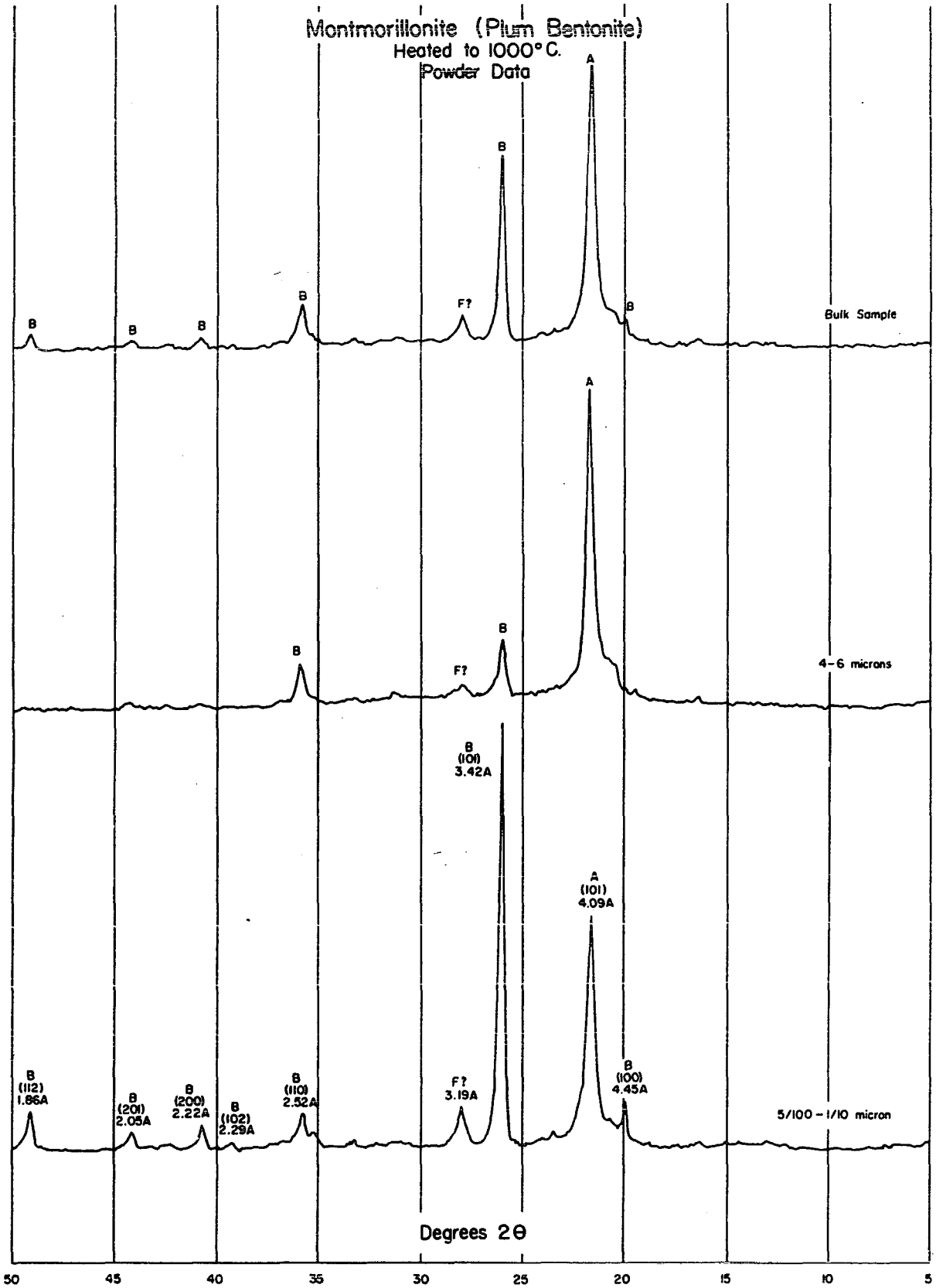

Figure 5. X-ray diffractometer scans of fired samples of Plum bentonite. (A) α-cristobalite, (B) β-quartz, (F) feldspar.

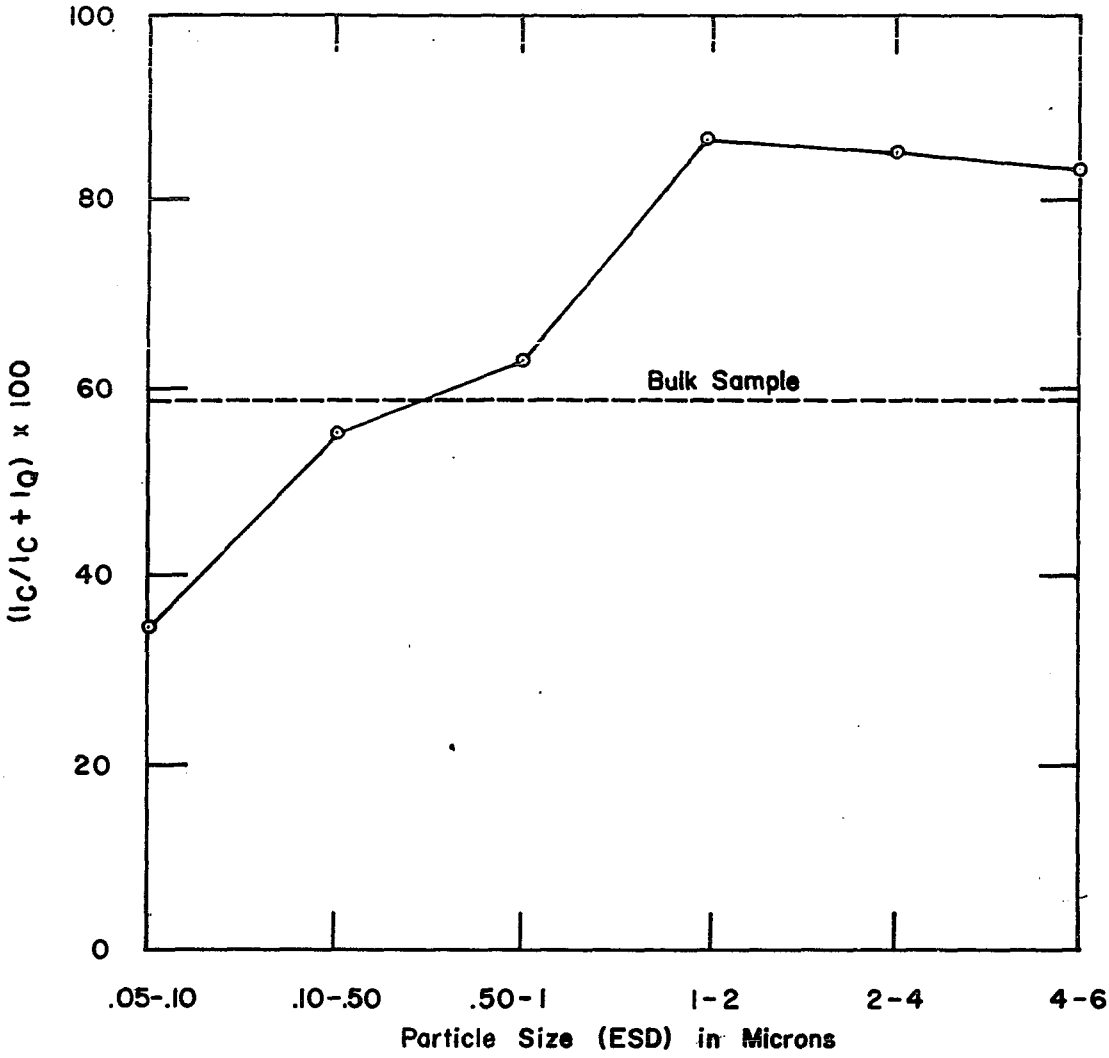

Figure 6. Relative intensity of alpha-cristobalite (101) peak (I_C) with respect to the sum of the intensities of the alpha-cristobalite (101) peak and the beta-quartz (101) peak (I_C+I_Q). Intensities are the result of peak height measurements on powder diffractograms of fired samples of Plum bentonite.

of this phase is directly proportional to the higher montmorillonite content in the small size fractions.

Chemical Analyses

Chemical analyses by x-ray fluorescence provided quantitative information concerning the elements silicon, aluminum, iron, magnesium, titanium, calcium, and potassium. Table 3 contains the chemical data on an air-dry basis.

TABLE 3

CHEMICAL ANALYSES OF THE SIZE-FRACTIONED PLUM BENTONITE

	Bulk	4-6	2-4	1-2	1/2-1	1/10-1/2	5/100-1/10
SiO_2	64.75	69.51	69.76	69.63	61.99	58.48	58.58
Al_2O_3	11.84	10.09	9.90	10.14	12.28	13.49	12.97
TiO_2	0.23	0.18	0.19	0.21	0.26	0.29	0.28
Fe_2O_3*	0.34	0.26	0.26	0.27	0.38	0.41	0.41
MgO	2.74	2.24	2.49	2.68	3.03	3.08	3.21
CaO	1.66	1.28	1.32	1.35	1.76	1.89	1.97
K_2O	0.12	0.12	0.12	0.36	0.38	0.38	0.39
H_2O^+	4.16	3.49	3.61	3.74	4.63	4.88	4.85
H_2O^-	11.66	10.14	10.10	9.09	12.55	14.30	14.57
Total	97.50	97.31	97.75	97.47	97.26	97.20	97.23

*All iron reported as Fe^{+3}.

These indicate an abundance of SiO_2 in the coarser fractions and a decrease of this constituent in the finer materials.

Structure

An attempt was made to partition the constituents into the tetrahedral, octahedral, and interlayer positions of the montmorillonite lattice using a technique described by Marshall (1949). Such calculations, however, resulted in an excess of silica that could not be accommodated by the tetrahedral positions. This also resulted in an octahedral cation deficiency. From x-ray diffraction it was determined that the montmorillonite is dioctahedral (b = 8.97Å) and the only other detectable phase is alpha-cristobalite. Assuming an ideal two-ion octahedral population (half unit-cell formula) all of the aluminum, iron, magnesium, and titanium were placed in the octahedral layer. The sum of the gram-atoms of these constituents was multiplied by a factor which brought the total number up to two ions. The number of gram-atoms of silicon was also multiplied by this factor and four of these placed in the tetrahedral positions. The excess silicon was reconverted to SiO_2 in the chemical analyses. The excess silica, as calculated for the bulk sample and all particle size fractions, is shown graphically in Figure 7. The amount of free SiO_2 is shown to vary from about 20 to 43 percent with the bulk sample estimated at 31.63 percent (oven-dry basis). These are minimum estimates because the maximum amount of silicon was allotted to the tetrahedral layer. Any substitution of aluminum for silicon in the tetrahedral layer would necessarily increase the excess of SiO_2 estimate.

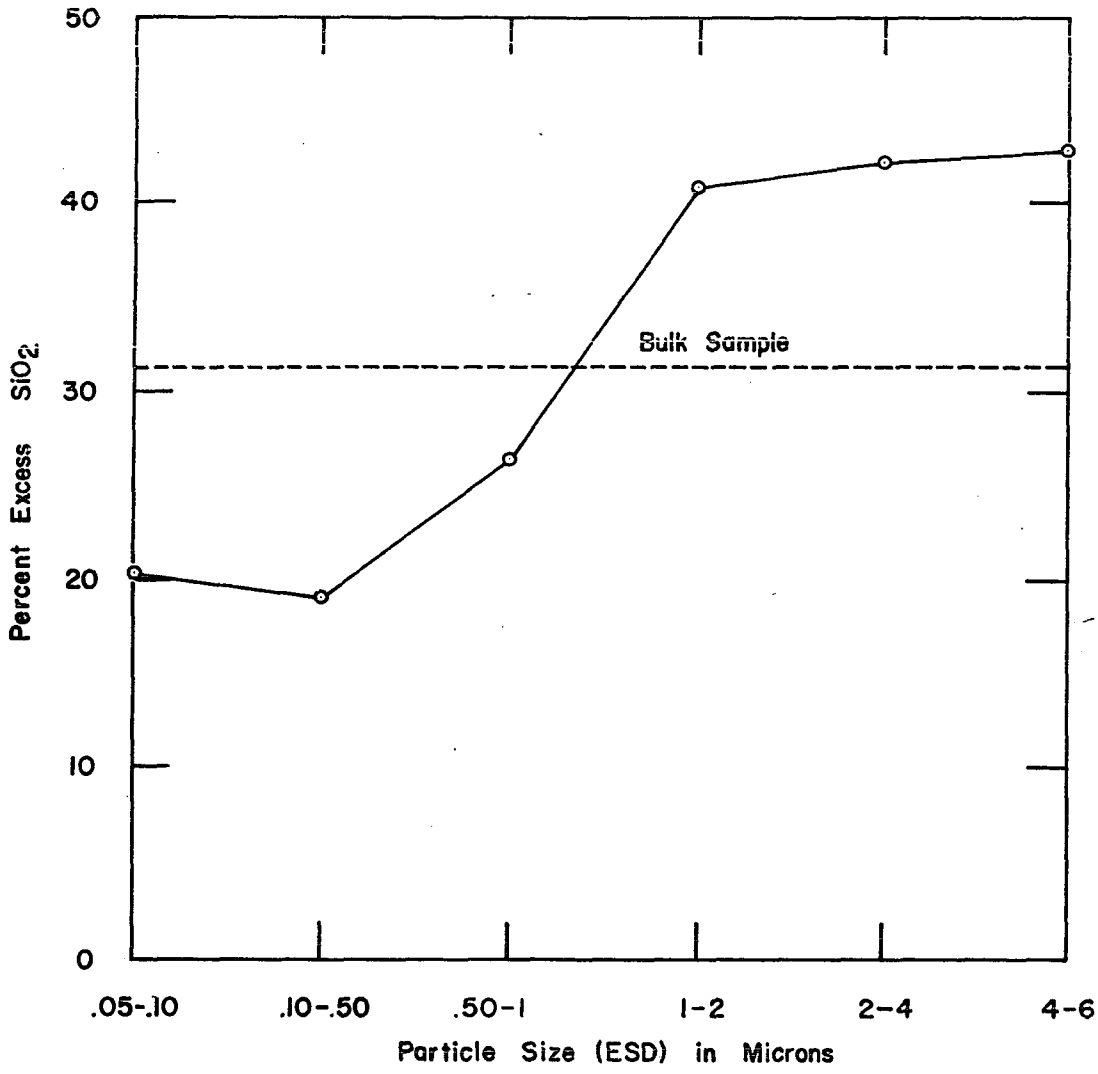

Figure 7. Percent of SiO_2 (on oven dry basis) estimated as an excess of the maximum SiO_2 that can be attributed to the montmorillonite phase of the size-fractioned Plum bentonite.

Table 4 lists the data resulting from this type of structure calculation for the bulk sample and all size fractions.

TABLE 4

STRUCTURAL DATA FOR THE PLUM BENTONITE MONTMORILLONITE*

	OCTAHEDRAL				INTERLAYER		EXCESS SiO_2
	Al	Mg	Fe	Ti	Ca	K	Wt. Percent Dry Basis
Bulk	1.511	.442	.0280	.0190	.193	.017	31.63
4-6	1.528	.429	.0251	.0173	.177	.021	42.90
2-4	1.484	.473	.0249	.0180	.180	.019	42.56
1-2	1.465	.491	.0251	.0192	.178	.057	40.84
1/2-1	1.486	.464	.0298	.0205	.194	.050	26.48
1/10-1/2	1.513	.437	.0293	.0208	.193	.047	19.32
5/100-1/10	1.485	.465	.0298	.0205	.206	.048	20.49

*Tetrahedral composition taken as Si_4 on half unit-cell basis.

The relative amounts of estimated excess SiO_2 agrees with the relative abundance of alpha-cristobalite as interpreted from x-ray diffraction and differential thermal analyses. However, there is an anomaly in the estimated percentage of free silica for the 1/10-1/2 micron fraction. The value of 19.32 percent excess SiO_2 seems to be too low with respect to that of the smaller 5/100-1/10 micron fraction (20.49 percent). Assuming a conservative estimate of 21 percent excess silica for this sample and computing the structural formula with a Marshall calculation results in a formula that shows a substitution of

0.04 ions of aluminum for silicon in the tetrahedral layer. This effect did not cause a significant deviation in the octahedral or interlayer composition as shown in Table 4.

Cation Exchange Capacity

The cation exchange capacity was determined by the titration method on one gram samples of the 1/2-1, 1/10-1/2, and 5/100-1/10 micron (ESD) fractions of the Plum Bentonite. Total exchange was taken at a pH of 7.0. Measurements were made in triplicate for all samples and maximum deviations from the average value for the same sample were less than two percent. The titration curves, shown in Figure 8, are plotted as pH versus meq NaOH per 100 grams of clay dried at 170° C. These are the results of averages of the three separate titrations for each sample. Table 5 lists the CEC of

TABLE 5

CATION EXCHANGE CAPACITY OF PLUM BENTONITE MONTMORILLONITE*

Actual	1/2-1μ	1/10-1/2μ	5/100-1/10μ
Measured	90.5	93.5	97.5
Calculated	81.5	88.9	92.5
Adjusted for Excess Silica			
Measured	123.	118.	123.
Calculated	111.	113.	116.
Excess SiO_2	26.48	21.00	20.49

*Reported as Meq NaOH per 100 gm. 170° C dry clay at pH of 7.0.

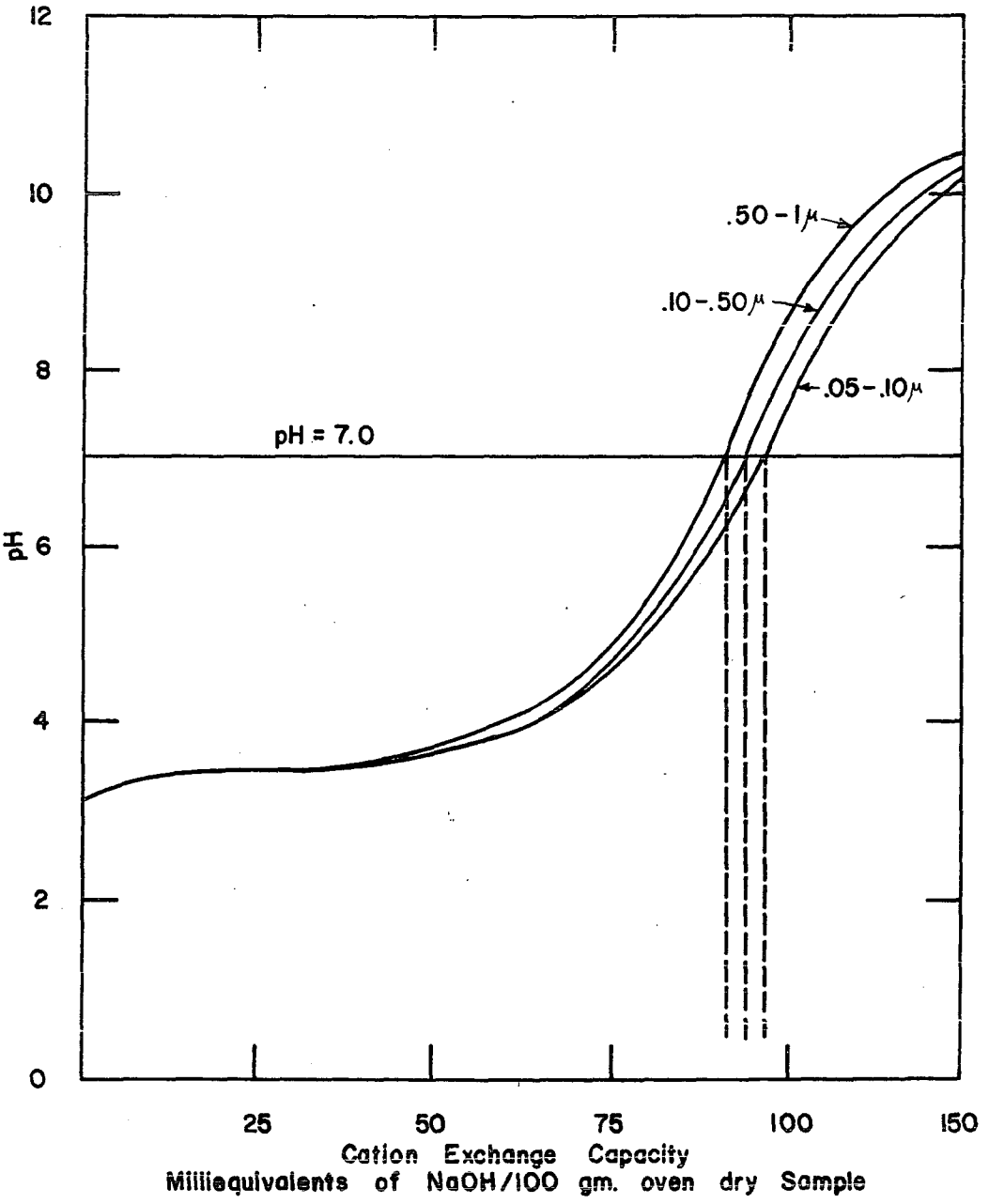

Figure 8. Titration curves for H-exchanged .05-.10, .10-.50, .50-1 micron fractions of the Plum bentonite.

the different size fractions and the theoretical values as calculated from the chemical analyses in Table 3. The calculated and measured CEC for each fraction are also shown after adjusting for estimated excess silica as listed in Table 4.

Difference in the calculated and measured cation exchange capacities may be due to several factors. The montmorillonite may contain some sodium, but an analysis for this constituent was not obtained. As little as 0.31 percent Na_2O dry basis would add another ten milliequivalents to the calculated exchange capacity. The finely divided alpha-cristobalite probably has a measureable exchange capacity, but it is thought thay any contributions from this constituent would be within the range of reproducibility of the analysis and, therefore, probably neglible.

The low adjusted exchange capacity for the 1/10-1/2 micron sample probably may be attributed to a low estimate for the excess silica. A higher estimate of twenty-four percent silica would increase the measured CEC to 123 meq per 100 gm. dry weight basis which is comparable to the values obtained for the other two fractions. This amount of excess silica would increase the calculated CEC to 117 milliequivalents.

Interpretations

Differences between the computed structural formulae of the 5/100-1/10 and 1/10-1/2 micron samples are not considered to be significant. The relative amounts of cristobalite

estimated for all samples are supported by x-ray and DTA data. The excess silica values, however, are minimum estimates. Adjustments in cation exchange capacities resulted in values for each size fraction which differed only within the range of reproducibility of the titration method employed. There is close agreement between calculated and measured CEC values. Thd calculated values are consistently low and may be due to the presence of a small amount of Na_2O for which analyses were not available. This may also account for the slightly lower interlayer cation charge with respect to the octahedral charge deficiencies.

Grim and Kulbicki (1961) analyzed forty montmorillonites by chemical, x-ray, DTA, diffractometer furnace, and optical methods. The results indicated that there are two distinct types of dioctahedral aluminum montmorillonites. Evidence is strongly opposed to a continuous isomorphous series and the end members were given the names Cheto- and Wyoming-types. Some samples that appeared at first to be intermediate types were partially separated on the basis of particle size into two distinct phases. The Cheto-type was concentrated in the coarser size fractions.

The Plum bentonite montmorillonite is necessarily classified as a Cheto-type. This is evident from the high magnesium for aluminum substitution in the octahedral layer. Cheto-type properties of the Plum bentonite montmorillonite are high CEC, DTA characteristics, especially in the high temperature region, and the formation of beta-quartz at 1000° C.

VERMICULITE

Llano Vermiculites

At least three genetically and mineralogically dissimilar vermiculites are found in Precambrian metamorphic rocks of the Llano uplift or near Llano, Texas (Barnes and Clabaugh, 1961). A pearly-white variety is found in a weathered marble associated with magnesite. Another type is best developed in a deposit on the Carl Moss Ranch and is associated with soapstone and talc. Hydrothermal activity has had a decisive influence on the formation of this vermiculite. The third type is brown vermiculite associated with the weathering of biotite in mica-amphibolite schist (Packsaddle schist, Paige, 1912). A detailed discussion of the geology, petrology, and occurrence of these vermiculites was provided by Clabaugh and Barnes (1959).

The vermiculite samples selected for the present study were collected at stop number twelve (Carl Moss Ranch) on the field trip led by Folk, and others (1961) as a part of the Tenth National Clay Conference. Two samples of vermiculite were collected. One type consisted of large books of yellowish brown crystals concentrated in veinlets. The average

crystal sizes are about one to two inches in diameter. The other sample was found as loose regolith material in which the individual crystal sizes range from about three millimeters down to clay-sized particles.

X-ray Diffraction Data

X-ray diffractometry data of a randomly oriented powder of the large yellowish-brown crystals (ground to 400 mesh) are listed in Table 6 and are compared with the x-ray data reported by Walker (1961) for Batavite and a vermiculite from West Chester, Pennsylvania. The chemical compositions of these three vermiculites are quite different, but are not indicated by differences in the x-ray diffraction powder data. Only a few of the weaker lines observed in the two samples reported by Walker were not observed in the Llano vermiculite (Carl Moss Ranch). In particular, attention is called to the d-spacing of the (060) lines from which the b-axis parameter may be calculated. This is 9.22 Å for Batavite and the West Chester vermiculite and 9.24 Å for the sample from the Carl Moss Ranch.

Powder data were also obtained for samples of the size-fractioned sample of vermiculite regolith. Figure 9 shows the diffractometer scans from ten to sixty-two degrees two-theta for the large crystals (ground to 400 mesh), 16-32, 1-2, and 5/100-1/10 micron samples. The powder data for the 16-32 micron fraction agrees well with the data listed in Table 7.

TABLE 6

X-RAY DATA FOR SELECTED WELL-CRYSTALLIZED VERMICULITE

INDICES	Batavite* d(Å)	Batavite* I est.	West Chester* Vermiculite d(Å)	West Chester* Vermiculite I est.	Llano Vermiculite Large Crystals d(Å)	Llano Vermiculite Large Crystals I/I_o x 100
002	14.4	vvs	14.4	vvs	14.39	100
004	7.18	vvw	7.20	vw	7.19	3
006	4.79	vw	4.79	vw	4.80	5
02*l* ; 11*l*	4.60	s	4.60	s	4.61	1
008	3.602	m	3.587	m	3.59	10
0,0,10	2.873	m	2.869	m	2.87	13
130; 200; 20$\bar{2}$	2.657	mw	2.657	mw	2.652	1
13$\bar{2}$; 20$\bar{4}$	2.602	ms	2.597	m	2.600	1
13$\bar{4}$; 202	2.550	m	2.550	mw	2.560	1
0,0,12; 13$\bar{6}$; 204	2.392	ms	2.392	ms	2.395	1
13$\bar{6}$; 20$\bar{8}$	2.277	vvw	2.266	vvw	-	-
13$\bar{8}$; 206	2.209	vvw	2.214	vw	2.204	1
138; 2,0,$\bar{10}$	2.082	w	2.081	w	2.083	1
0,0,14	-	-	2.048	vw	2.049	1
208	2.016	w	2.011	vw	2.016	1
1,3,$\bar{12}$; 2,0,10	1.835	vvw	1.835	vvw	1.833	1
2,0,$\bar{14}$	1.744	mw	1.748	w	1.745	1
1,3,$\bar{14}$; 2,0,$\bar{12}$	1.673	mw	1.677	mw	1.676	1
1,3,14; 2,0,$\bar{16}$	1.576	vvw	1.574	vvw	1.584	1
060; 1,3,$\bar{16}$; 2,0,14 330; 332; 334	1.537	s	1.537	ms	1.540	1

TABLE 6--Continued

INDICES	Batavite* d(Å)	Batavite* I est.	West Chester* Vermiculite d(Å)	West Chester* Vermiculite I est.	Llano Vermiculite Large Crystals d(Å)	Llano Vermiculite Large Crystals I/I_o x 100
332; $33\bar{6}$	1.506	vvw	1.508	vvw	-	-
0,0,20; 1,3,16; 2,0,18	1.444	vw	1.449	w	1.447	1
338	1.356	vw	1.357	vw	1.361	-
1,3,18; $2,0,\bar{20}$; $3,3,\bar{12}$; $40\bar{2}$	1.332	mw	1.334	mw	1.331	1
$2,0,\bar{20}$; 400; $40\bar{6}$	1.319	mw	1.320	mw	-	-
1,3,20; 2,0,18; 3,3,14; 402	1.296	w	1.298	w	1.294	-
404	1.278	w	1.275	vw	-	-

*After Walker (1961).

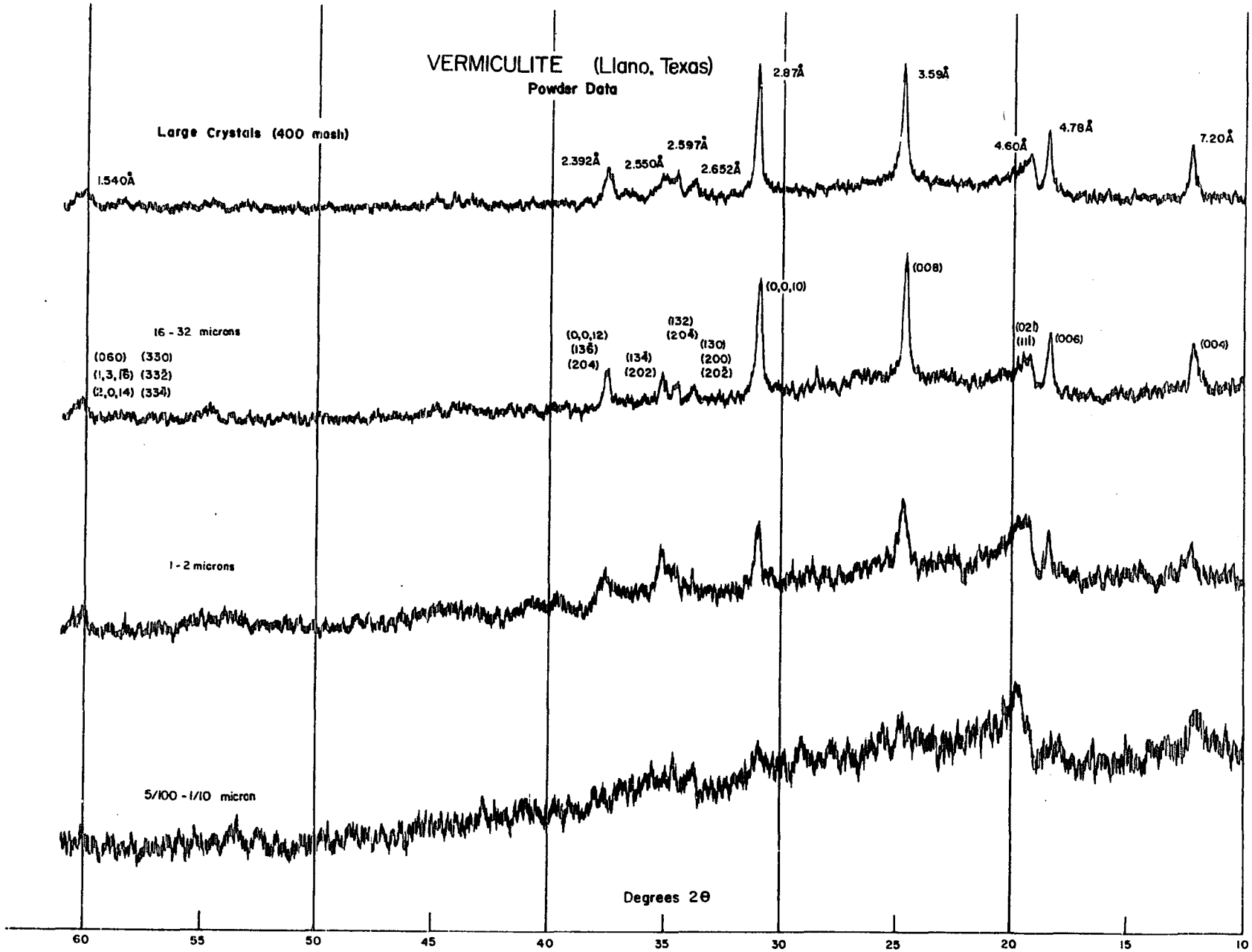

Figure 9. X-ray diffractometer scans of random orientations of selected Llano vermiculite samples.

TABLE 7

X-RAY DATA FOR SELECTED SAMPLES OF SIZE-FRACTIONED LLANO VERMICULITE

INDICES	Particle Size (Microns) 16-32 d(Å)	4-8 d(Å)	1-2 d(Å)	1/4-1/2 d(Å)
002	14.52	14.40	14.40	14.50
004	7.22	7.20	7.20	7.31
006	4.77	4.78	4.80	-
02ℓ; 11ℓ	4.61	4.61	4.69	4.50
008	3.60	3.59	3.60	3.60
0,0,10	2.890	2.862	2.878	2.89
130; 100; 20$\bar{2}$	2.656	2.636	2.648	-
132; 204	2.596	2.593	-	-
13$\bar{4}$; 202	2.557	2.553	2.550	2.564
0,0,12; 13$\bar{6}$; 204	2.397	2.392	2.392	-
138; 2,0,$\bar{10}$	2.084	-	-	-
0,0,14	2.058	-	-	-
208	2.020	-	-	-
1,3,$\bar{14}$; 2,0,12	1.680	-	-	-
060; 1,3,$\bar{16}$; 2,0,14; 330; 332; 334	1.537	1.537	1.535	-
0,0,20; 1,3,16; 2,0,$\bar{18}$	1.450	-	-	-
1,3,18; 2,0,$\bar{20}$; 3,3,12; 402	1.334	-	-	-

The differences are mainly the absence of some of the weaker diffraction lines. This loss of lines continues progresively through to the smallest size fraction. A significant change of d-spacings is not observed, however, until the particle size becomes less than one micron. This effect may be observed in the diffractometer traces of the 1-2 and 5/100-1/10 micron fractions and in the data listed in Table 7. In the

less than one micron fractions the (060) diffraction peak disappears. It does not shift to a higher two-theta value, thus giving no evidence for the presence of a dioctahedral phase. A shift of the (02), (11ℓ) peak from 19.3 to 19.7 degrees two-theta, however, strongly supports this possibility.

All size-fractions of the vermiculite were prepared as sedimented slides. An equal amount (0.05 grams) of each particle size was accurately weighed, dispersed in a few drops of distilled water, and all the dispersed material placed on glass slides. All the sedimented materials were humidified for eight hours and scanned on a diffractometer from two to ninety degrees two-theta.

A small amount of talc and phlogopite occurred in all size fractions down to one micron. Figure 10 shows the (00ℓ) oriented diffraction scans for the 16-32, 1-2, and 5/100-1/10 micron fractions. A total of eleven orders of the (002) d-spacing were observed on the 16-32 micron x-ray diffraction pattern. Finer fractions down to the less than one micron material have seven observable orders. For the finest fractions only five orders are present. A plot of the relative intensity (peak height basis) of six progressive orders of the (002) peak of 14.5 $\mathring{A}$ for some of the fractions is shown in Figure 11. In the finer fractions the relative intensities of the higher order reflections show a progressive decrease in intensity. In the finest fraction the relative intensities

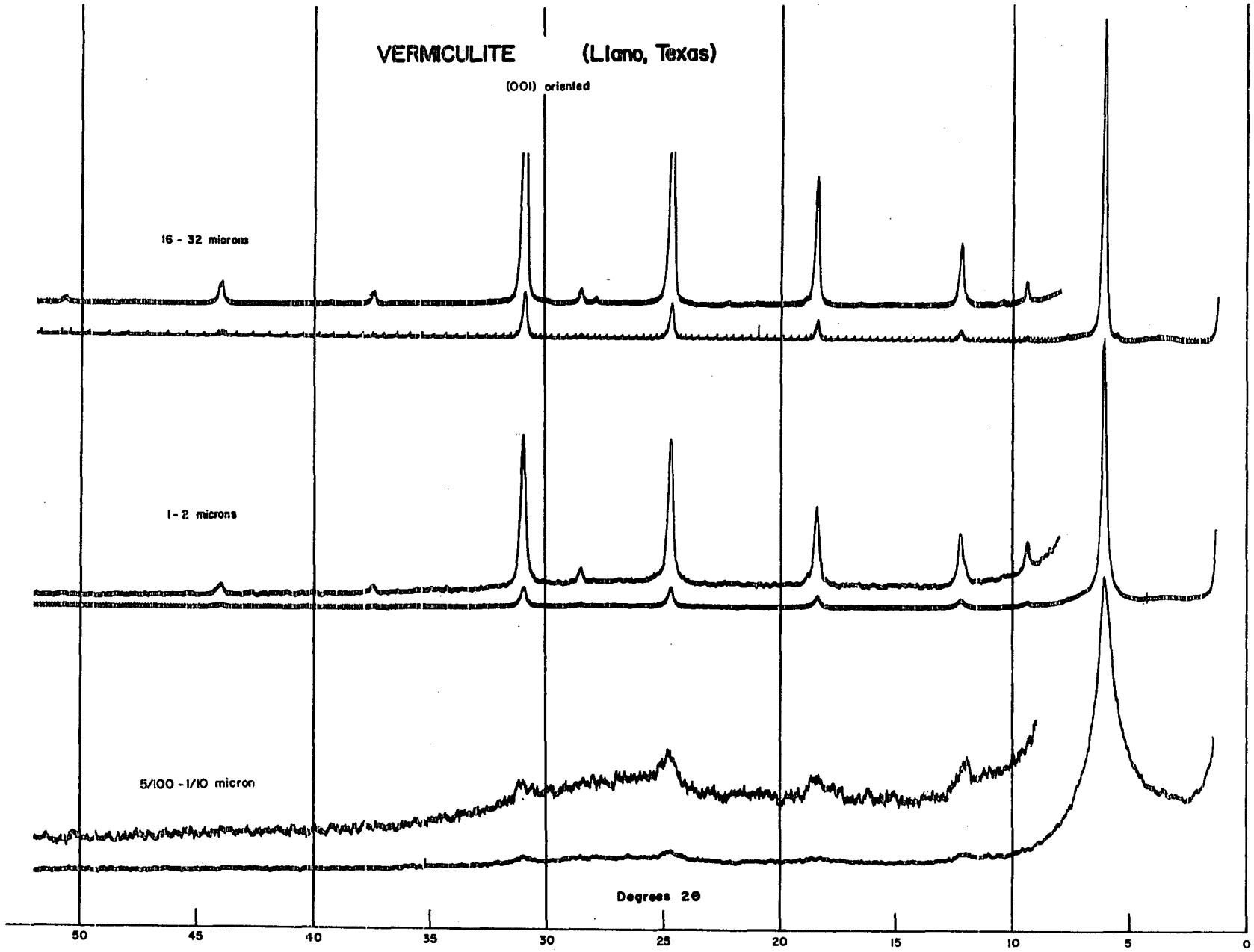

Figure 10. X-ray diffractometer scans of (00ℓ) orientations of selected Llano vermiculite samples.

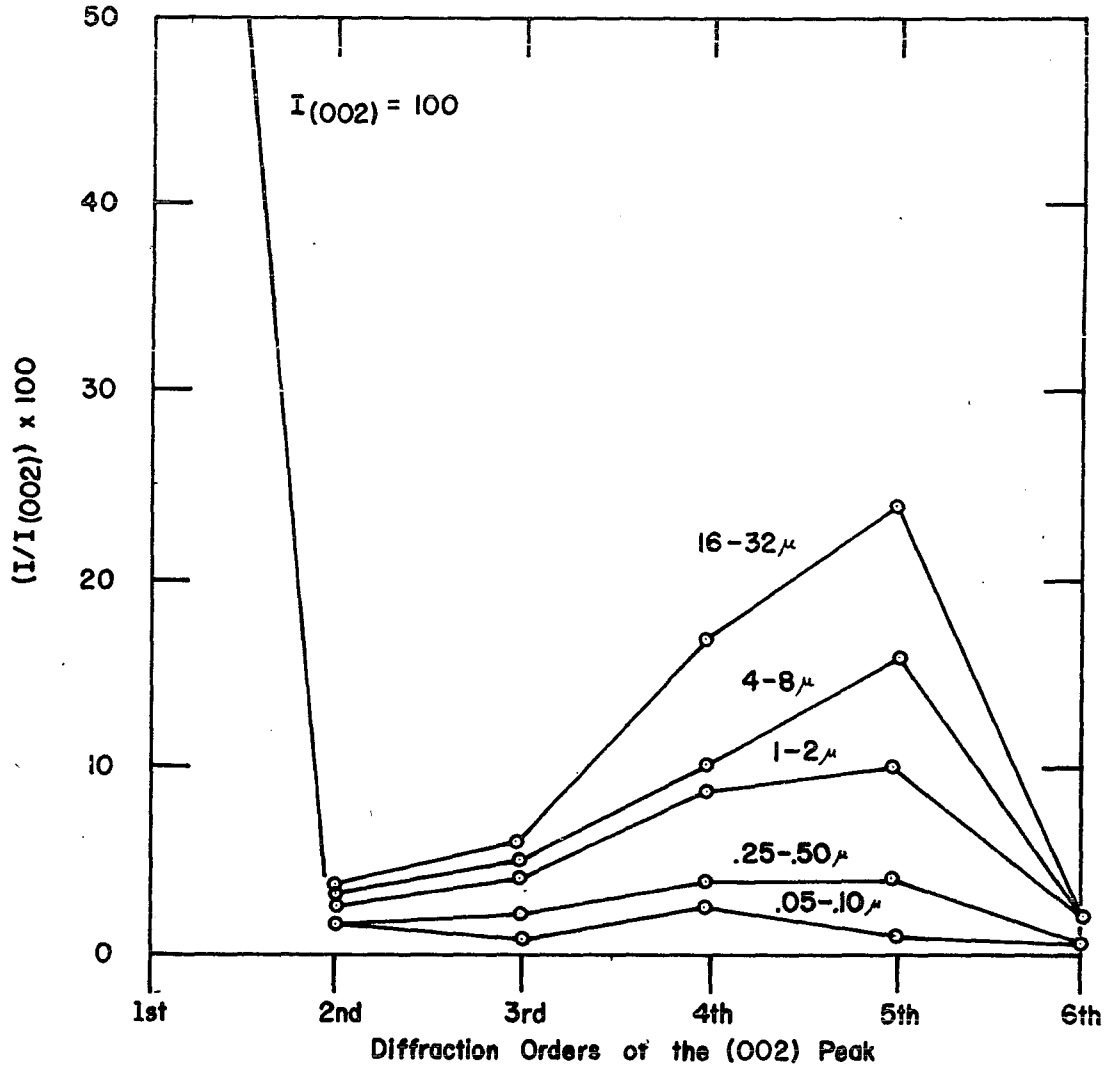

Figure 11. Relative intensities of orders of the (002) peaks for the size-fractioned Llano vermiculite. Based on peak height measurements of (00ℓ) oriented sample x-ray data.

of successive orders are not similar to the typical continuous increase from the (004) to the (0,0,10) of a true vermiculite.

The (00ℓ) oriented samples consisting of equal amounts of material (0.05 gm per slide) were scanned at the same scale factor, machine, diffractometer, and slit settings to compare the relative intensities of the (002) diffraction peak (at about 14.5 Å). Scans were also made at various scale factor settings which enhanced the (002) reflections so that they attained approximately the same peak height on their respective patterns. These latter were used to obtain an index of peak sharpness. Sharpness is observed to decrease from the coarser fractions through to the finer fractions. Relative intensities of the (002) peaks were determined by measuring the area under the curve and multiplying all values by a factor which would convert the intensity of the (002) of the 16-32 microns fraction intensity to 100. The ratio of peak height to peak width at half-height was used as an index of the degree of peak sharpness. Both the relative intensity of the (002) reflections calculated as:

$$I/I_{(16-32)} \times 100 \qquad 3$$

and the sharpness index:

$$R/R_{(16-32)} \times 100 \qquad 4$$

where R is the ratio of peak height to peak width at half-height for a particular size fraction are shown graphically in Figure 12. The relative intensities of the (002) peaks

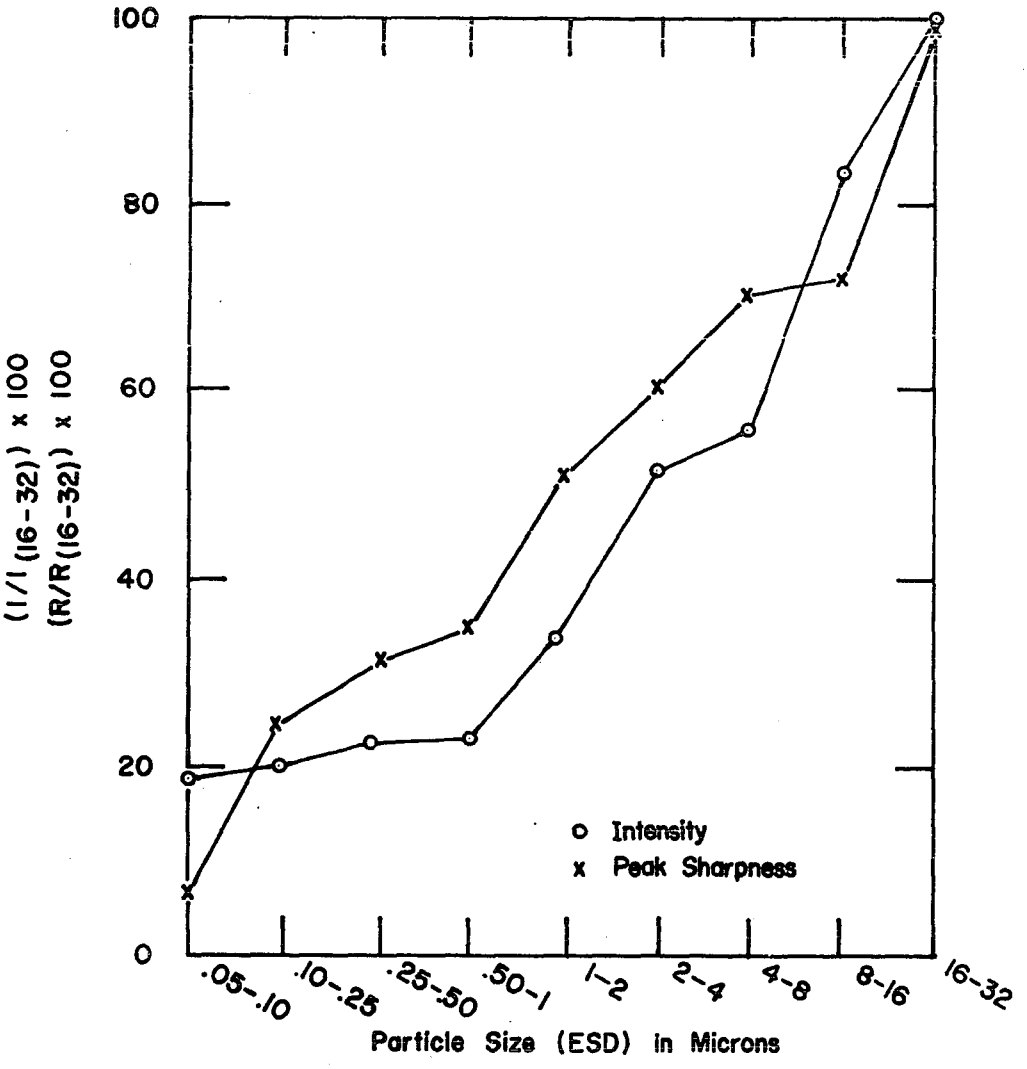

Figure 12. Relative intensity $I/I_{(16-32)}$ x 100 and peak sharpness index $R/R_{(16-32)}$ x 100 where $\underline{R}$ is the ratio of the peak height to peak width at half-height for the (002) diffraction peaks of each particle size fraction of the Llano vermiculite.

show a progressive decrease with decreasing particle size down to the one micron material. The finer fractions, 1/2-1, 1/4-1/2, 1/10-1/4, and 5/100-1/10 micron fractions have a relative intensity of about 20-25 percent that of the 16-32 microns fraction. The index of peak sharpness also decreases with particle size and does so regularly through to the finest fractions (5/100-1/10 micron). The increase in line broadening is partially a reflection of the decrease in crystalline order of the finer materials. It is also a function of the decrease in the particle size. The decrease in relative intensity of the (002) peak is a function of the crystallinity of the material and also can be a function of the lattice chemistry.

The same slides that were used in the (00ℓ) oriented scans were subjected to ethylene glycol treatment. The slides were placed in an atmosphere saturated with ethylene glycol vapor at 60° C and a minimum of eight hours was allowed for complete expansion. X-ray diffractometry was carried out from two to sixty-five degrees two-theta. Check scans were made over the (002) peak after a complete run to make sure that a collapse of the expanded material had not occurred during the time the complete scan was being made.

The 5/100-1/10 micron fraction undergoes an almost complete expansion to 16.5 Å. A slight shoulder on the peak at about six degrees two-theta also suggests that some material

did not undergo ethylene glycol expansion. This becomes more apparent in the coarser particle size fractions. Figure 13 shows the diffractometer traces for the 16-32, 1-2, and 5/100-1/10 micron fractions. Successive orders show that the ethylene glycol expansion in the coarser fractions is variable and at least two and perhaps three different equilibrium d-spacings or degrees of swelling are present. In most cases the various (002) peaks were not resolved in the five to six-degree range, but are observed as a single peak occurring at about 5.5 degrees two-theta (16.1 Å).

An approximation of the percent of expandable material present in each size-fraction was made by measuring the decrease in the height of the 14.5 Å peak after ethylene glycol treatment. The results of these data are plotted in Figure 14 as percent decrease in intensity of the (002) peak versus particle size. This indicates that the percent of expandable material varies from 87 percent in the 0.05 to 0.10 micron fraction to 30 percent in the 16-32 microns fraction.

Differential Thermal Analysis

Figure 15 contains the DTA curves of all samples run at 10° C per minute from room temperature to 1020° C. All samples have an endothermic doublet in the 100-250° C range. This doublet marks the loss of interlayer water and is not well resolved in the finer fractions as in the coarser materials. The endotherms at 500-600° C and at 700-900° C indicate

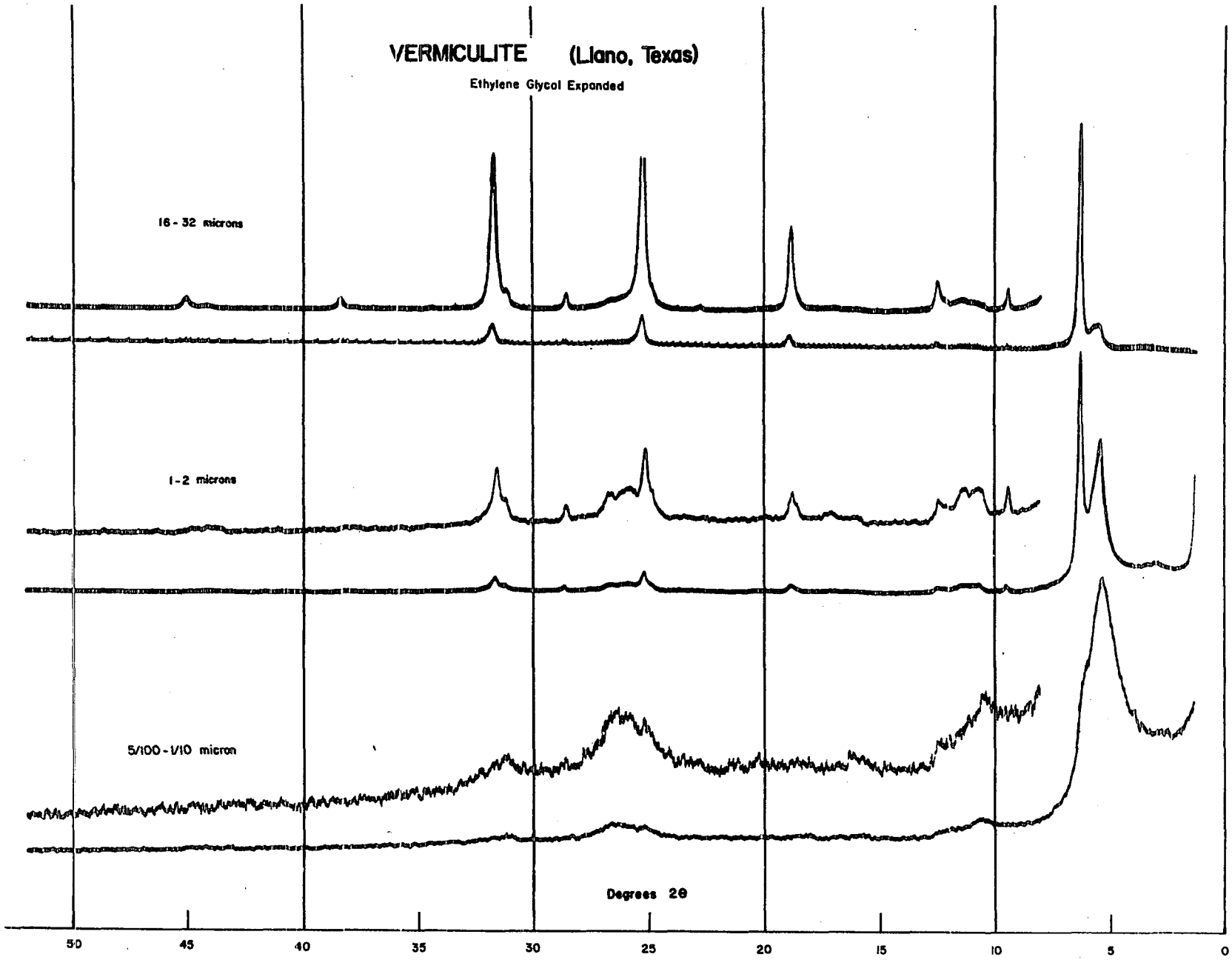

Figure 13. X-ray diffractometer scans of ethylene glycol expanded Llano vermiculite samples.

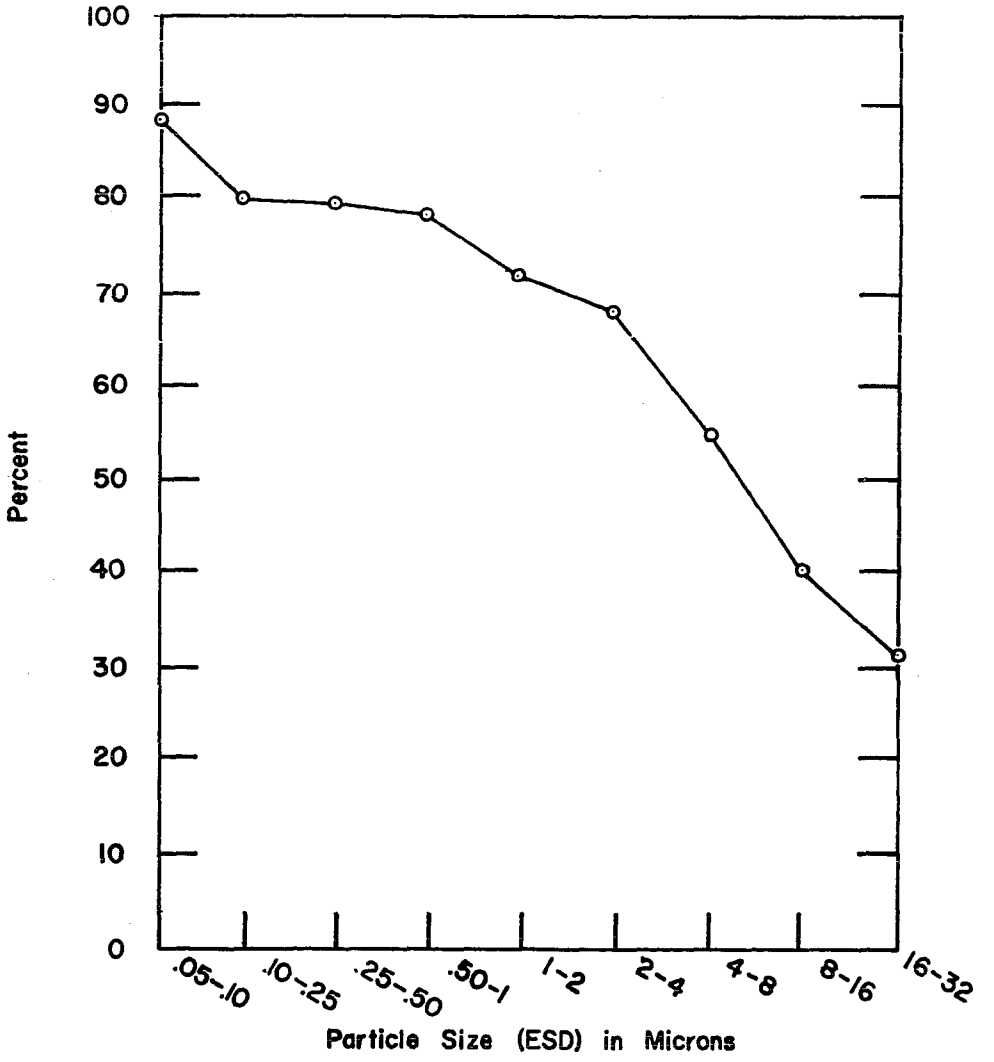

Figure 14. Percent reduction in height of the (002) peak of size-fractioned vermiculite samples after ethylene glycol treatment.

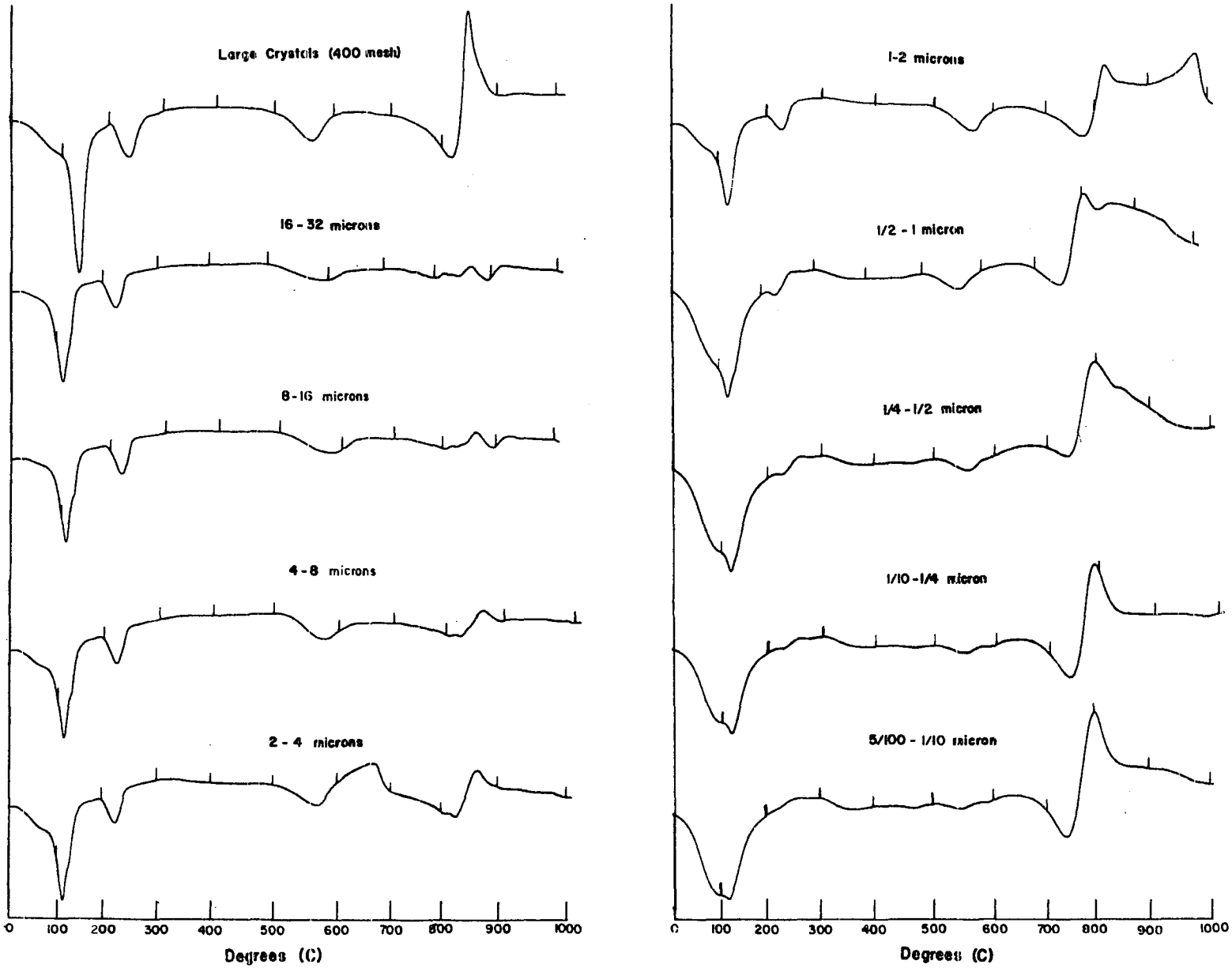

Figure 15. Differential thermal analysis patterns of Llano vermiculite samples.

the loss of water due to a breakdown of the octahedral cation to hydroxyl bond. The endotherms at 800-900° C represent the formation and appearance of non-clay mineral high temperature phases.

All samples were heated at 1000° C for twelve hours in a high temperature furnace. After firing, the samples were cooled to room temperature and x-ray diffractometer scans were run on the powdered materials. The high temperature phases that formed were the same for all fractions and for the large crystals. The dominant phase is clinoenstatite with some alpha-Fe_2O_3 (hematite) observed in the finer fractions. Figure 16 shows the diffractometer traces of the fired samples of the large crystals (ground to 400 mesh), 16-32, 1-2, and 5/100-1/10 micron samples. The clinoenstatite (CE) and hematite (H) diffraction peaks are labeled.

Chemical Analyses

Partial quantitative chemical analyses were obtained by x-ray fluorescence techniques. The results are listed in Table 8 and compared with two analyses of vermiculite from the same locality provided by Barnes and Clabaugh (1961) which were analyzed by the Minnesota Rock Analysis Laboratory, Minneapolis. The agreement is fairly reasonable, considering that the analyses were not run on cuttings of the same material. Analysis by x-ray fluorescence of the large crystals (ground to 400 mesh) shows a higher silica and iron oxide content and

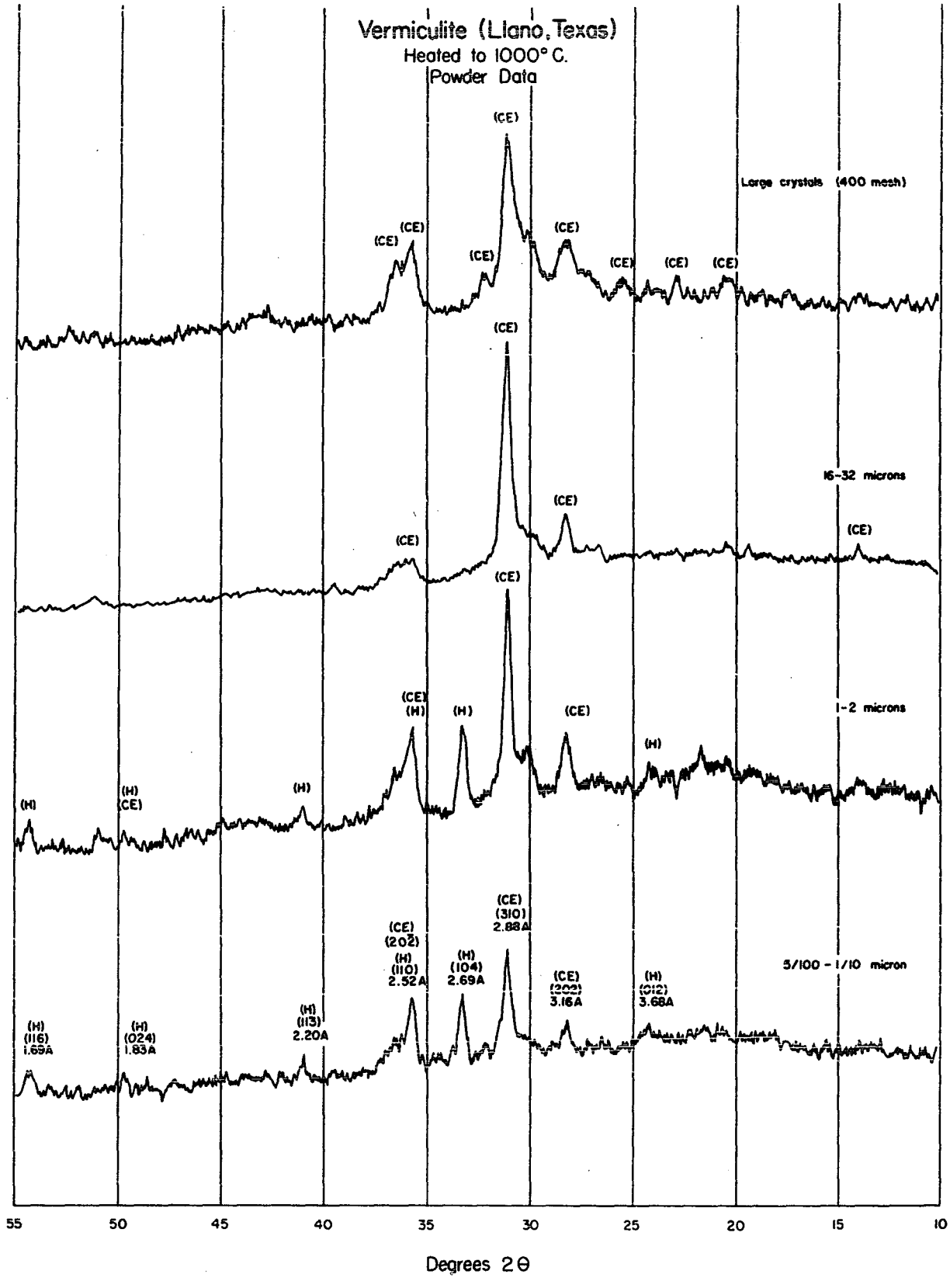

Figure 16. X-ray diffractometer scans of fired samples of Llano vermiculite. (CE) clinoenstatite, (H) hematite.

TABLE 8

CHEMICAL ANALYSES OF LLANO VERMICULITES (CARL MOSS RANCH)

	Guidebook*		Analyses by X-ray Fluorescence								
	Sample 1	Sample 2	Sample A	B-1	B-2	B-3	B-4	B-5	B-6	B-7	B-8
SiO_2	35.19	34.95	39.03	40.96	41.50	41.82	42.16	42.07	43.67	44.33	44.27
Al_2O_3	12.73	12.85	9.16	8.45	8.16	8.18	8.18	8.13	8.39	8.20	8.13
TiO_2	0.75	0.13	1.03	0.50	0.54	0.54	0.55	0.51	0.42	0.42	0.37
Fe_2O_3	3.52	3.09	4.95	6.49	6.96	7.87	8.59	9.60	12.91	13.79	13.75
FeO	0.46	0.57	-	-	-	-	-	-	-	-	-
MnO	0.05	0.03	-	-	-	-	-	-	-	-	-
MgO	26.85	29.25	24.01	22.31	21.93	20.01	18.68	15.70	10.47	8.99	9.22
CaO	0.24	0.00	0.11	0.57	0.56	0.43	0.41	0.39	0.41	0.44	0.45
Na_2O	0.02	0.02	-	-	-	-	-	-	-	-	-
K_2O	0.01	0.03	0.05	0.09	0.17	0.20	0.21	0.20	0.30	0.32	0.35
H_2O^+	10.77	10.87	9.55	8.55	8.42	8.88	10.18	9.89	9.97	9.91	9.85
H_2O^-	9.00	7.55	10.14	9.72	9.62	9.65	8.53	10.76	10.78	10.81	10.75
F	0.15	0.38	-	-	-	-	-	-	-	-	-
Cl	0.04	-	-	-	-	-	-	-	-	-	-
Total	99.78	99.72	98.03	97.73	97.86	97.58	97.49	97.25	97.32	97.21	97.14

*From Barnes and Clabaugh (1961).

Legend: Sample A refers to the large yellow crystals that were ground to 400 mesh. Samples B refer to the size-fractioned vermiculite, particle sizes 16-32 (B-1), 8-16 (B-2), 4-8 (B-3), 2-4 (B-4), 1-2 (B-5), 1/2-1 (B-6), 1/4-1/2 (B-7), and 1/10-1/4 (B-8) microns (ESD).

a lower magnesia and alumina content than the two analyses from the guidebook. Analyses of the size-fractioned material indicate a progressive increase of SiO_2, Fe_2O_3, and K_2O, and a decrease in the MgO content from the coarser (16-32 microns) to the finer (1/10-1/4 micron) fractions. Variations in Al_2O_3 are considered within the range of accuracy of the x-ray fluorescence techniques. Analyses of Na_2O, MnO, F, and Cl were not determined by x-ray fluorescence, and all iron was reported as Fe_2O_3. Figure 17 is a graphical illustration of the analyses listed in Table 8 calculated on the basis of weight percent of oxides on a 1000° C fired basis. Only the oxides of the more significant constituents, silicon, aluminum, iron, and magnesium, are included.

Structure

The various chemical constituents from the analyses reported in Table 8 were partitioned into a three-layer mica lattice using the method described by Marshall (1949). The results are listed in Table 9 on a half unit-cell formula basis (22 charges). There were no available means of determining the relative ratio of ferric to ferrous iron present, therefore, calculations were made twice. Row 1 considers all iron as Fe^{+3} and Row 2 considers all iron as Fe^{+2}. From the analyses provided by Barnes and Clabaugh (1961) listed in Table 8, the iron seems to be predominantly in the higher oxidation state and it is thought that calculations on this basis

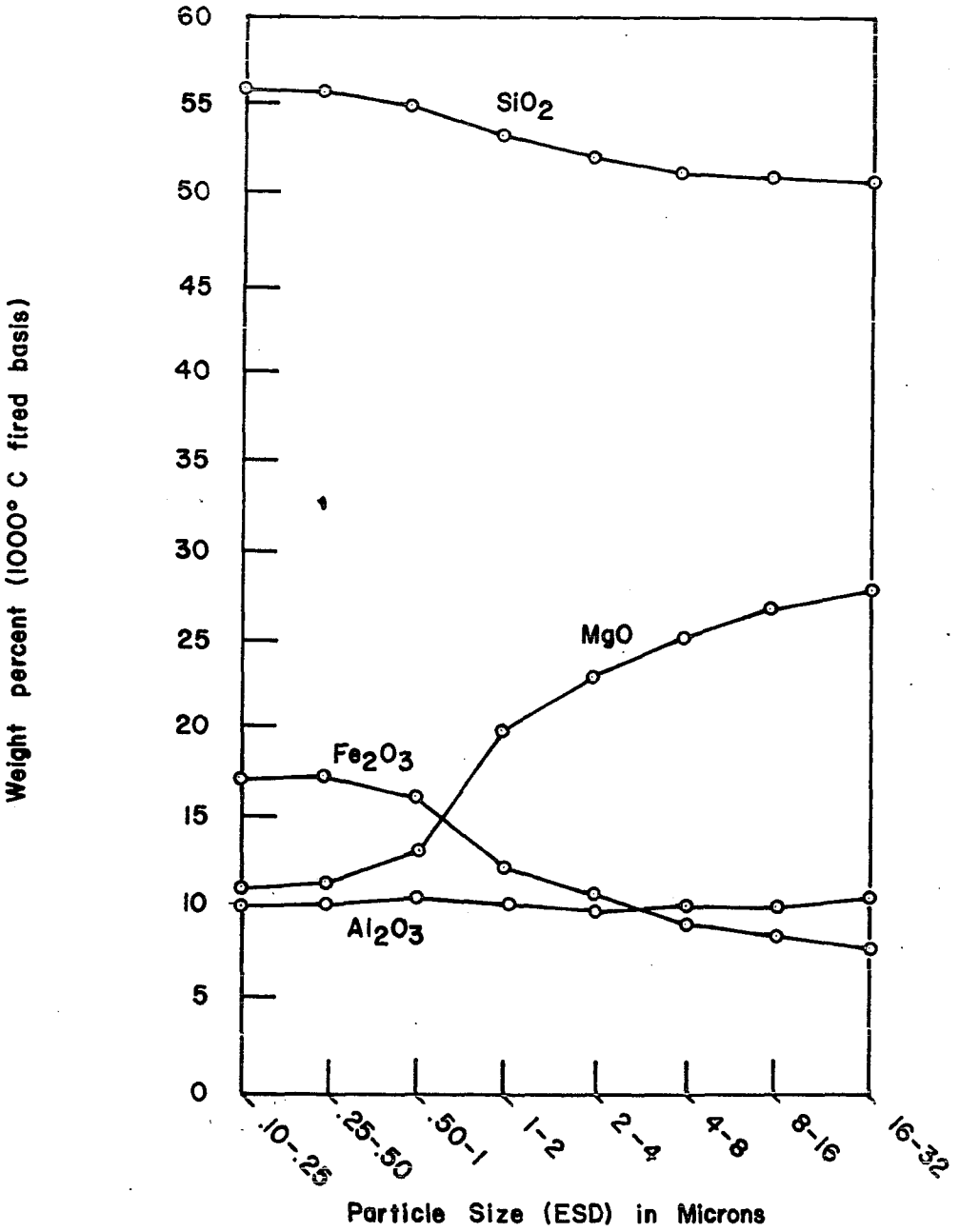

Figure 17. Partial chemical data on size-fractioned vermiculite. Based on quantitative analyses by x-ray fluorescence.

TABLE 9

RESULTS OF STRUCTURE CALCULATIONS ON CHEMICAL ANALYSES OF THE SIZE-FRACTIONED LLANO VERMICULITE

ESD	*	Tetrahedral Si	Tetrahedral Al	Octahedral Mg	Octahedral Fe	Octahedral Al	Octahedral Ti	Number Octahedral Cations	Interlayer Cations Mg	Interlayer Cations Ca	Interlayer Cations K
16-32	1	3.24	.76	2.31	.38	.04	.03	2.77	.32	.05	.01
	2	3.30	.70	2.38	.39	.11	.03	2.91	.30	.05	.01
8-16	1	3.27	.73	2.28	.41	.03	.03	2.75	.30	.05	.02
	2	3.34	.66	2.36	.41	.11	.03	2.90	.27	.05	.02
4-8	1	3.33	.67	2.09	.47	.10	.03	2.69	.28	.04	.02
	2	3.40	.60	2.19	.48	.18	.03	2.88	.25	.04	.02
2-4	1	3.37	.63	1.95	.52	.14	.03	2.64	.27	.04	.02
	2	3.45	.55	2.05	.53	.24	.03	2.85	.23	.04	.02
1-2	1	3.45	.55	1.69	.59	.24	.03	2.55	.23	.04	.02
	2	3.55	.45	1.79	.61	.36	.03	2.79	.18	.04	.02
1/2-1	1	3.60	.40	1.18	.80	.41	.03	2.37	.15	.04	.02
	2	3.73	.27	1.24	.83	.58	.03	2.68	.09	.04	.03
1/4-1/2	1	3.66	.34	.97	.85	.45	.03	2.31	.13	.04	.03
	2	3.80	.20	1.10	.89	.63	.03	2.65	.05	.04	.04
1/10-1/4	1	3.65	.35	1.02	.85	.44	.02	2.33	.11	.04	.03
	2	3.80	.20	1.14	.89	.62	.02	2.67	.04	.04	.03

*1 = Fe^{+3}; 2 = Fe^{+2}.

represent a closer approximation to the actual structural formula. Structural formulae are also written on the assumption that the octahedral layer does not contain more than six positive charges (half unit-cell basis). This assumption may not be strictly valid, but it provides a common basis for directly comparing the calculated structural formulae of the various particle sizes.

The data in Table 9 indicate that the aluminum for silicon substitution in the tetrahedral layer decreases with decreasing particle size with a relative increase in the aluminum and iron content with respect to magnesium. The titanium content is relatively constant throughout the range of particle sizes. The total surface charge and interlayer cation contents is also observed to decrease with the size of the particles. This is predominantly a function of the variation in interlayer magnesium. The calcium and potassium contents are relatively constant on an ion for ion basis.

The data in Table 9 have been plotted graphically in Figures 18, 19, and 20, for ease of examination. Figure 18 graphically shows the variation in the Al/Si ratio versus particle size. For comparison purposes dashed lines have been added which show the Al/Si ratio for Batavite and a vermiculite from West Chester, Pennsylvania, provided by Walker (1961). Also represented by dashed lines are the results of Marshall calculations on the analysis of sample 1 (from the guidebook), and the large crystals of Llano vermiculite from the Carl Moss

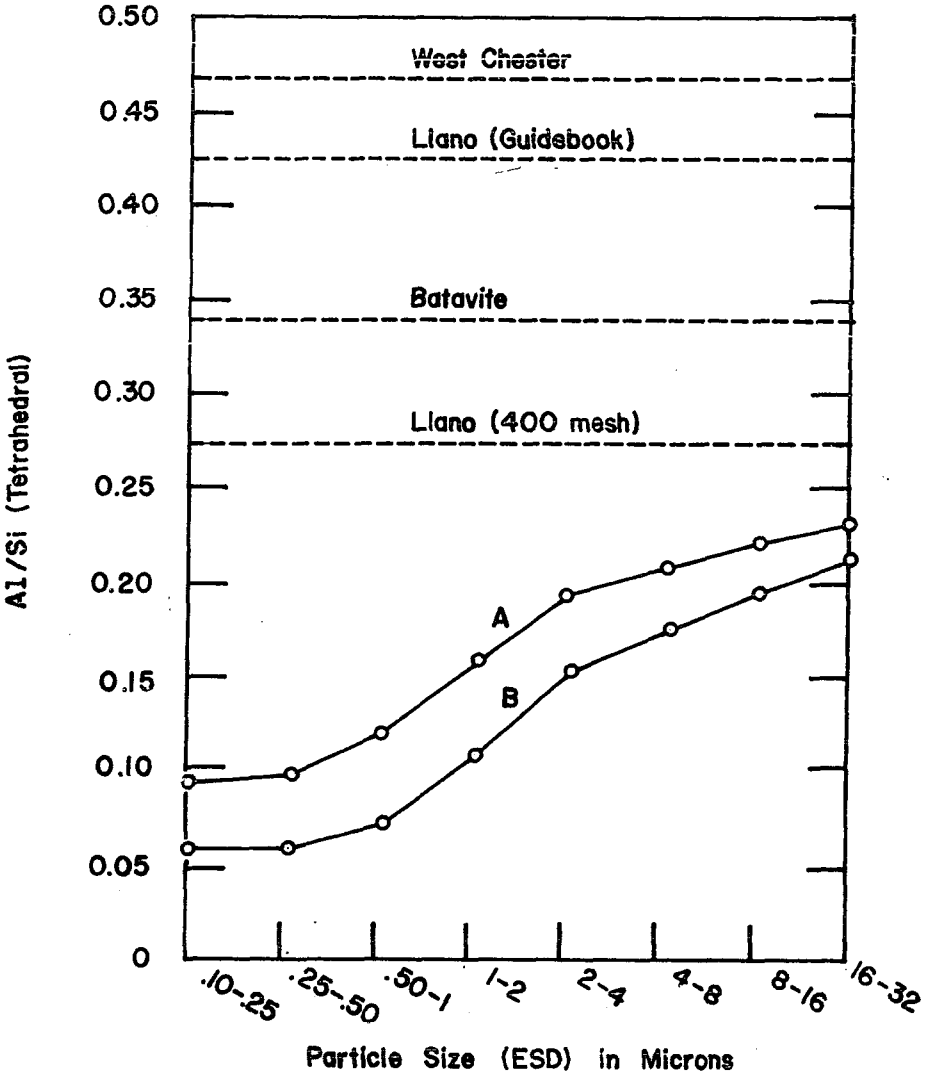

Figure 18. Tetrahedral layer compositions of selected vermiculites and size-fractioned Llano vermiculite.

Curve A: all iron considered as Fe^{+3}.
Curve B: all iron considered as Fe^{+2}.

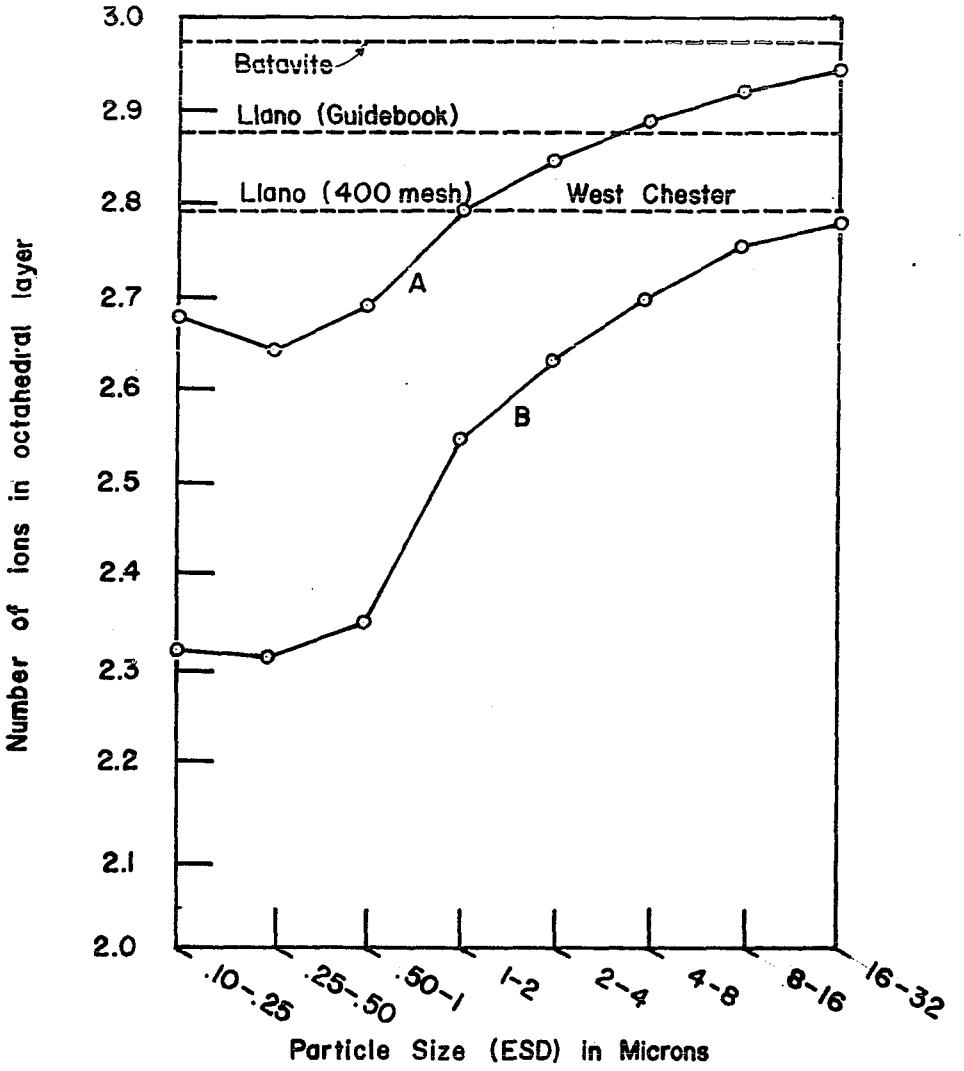

Figure 19. Total ion content of octahedral layer of selected vermiculites and size-fractioned Llano vermiculite.

Curve A: all iron considered as Fe^{+2}.
Curve B: all iron considered as Fe^{+3}.

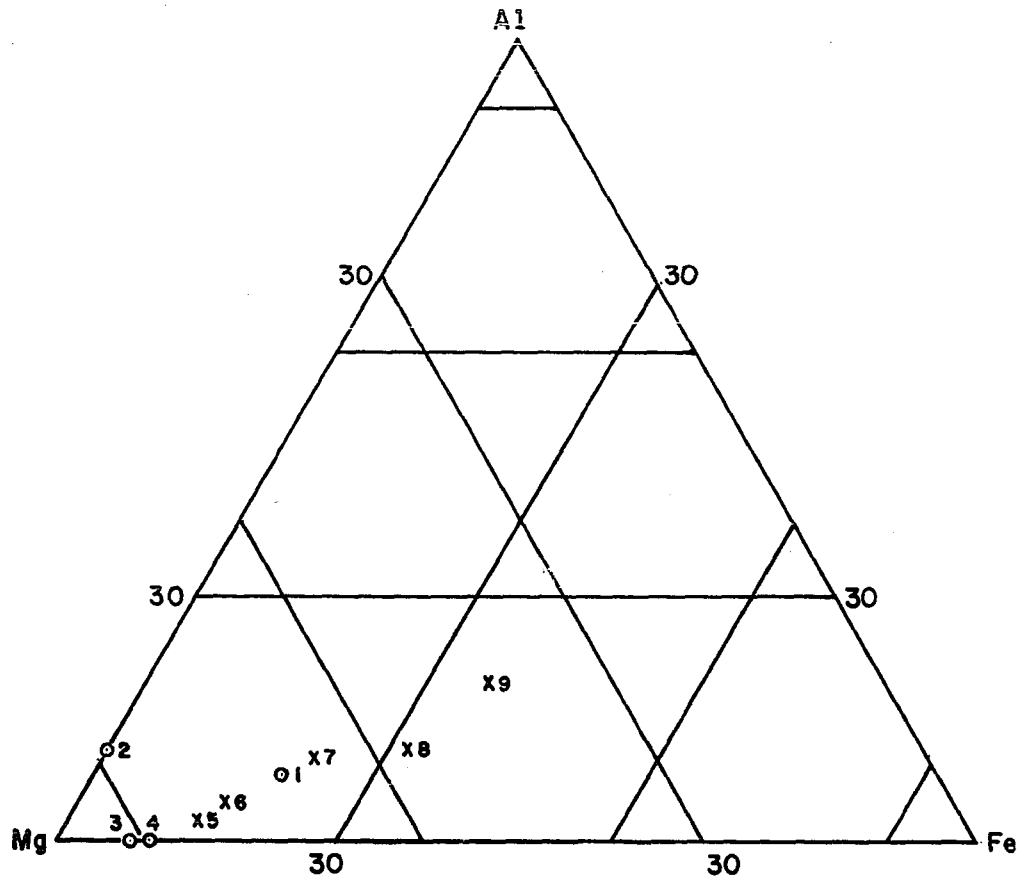

Figure 20. Octahedral layer population of selected vermiculites.

1. West Chester
2. Batavite
3. Llano (Guidebook)
4. Llano (400 mesh)

5-9. Size-fractioned Llano vermiculite
- (5) 16-32 microns
- (6) 4-8 microns
- (7) 1-2 microns
- (8) 1/2-1 micron
- (9) 1/10-1/4 micron

Ranch which were ground to 400 mesh and analyzed by x-ray fluorescence techniques. Curve A represents the results of structure calculations with all iron considered as Fe^{+3} and Curve B, in which all iron is taken as Fe^{+2}.

Figure 19 is a graphical illustration of the total ion content in the octahedral layer. Again Batavite, West Chester, Llano (guidebook analysis) and Llano (400 mesh, x-ray fluorescence data) vermiculites are represented by dashed lines. Curve A represents the results of calculations in which all iron is considered as Fe^{+2}, whereas, in Curve B the iron is considered as all Fe^{+3}.

Figure 20 is a triangular plot showing the contribution of each ionic constituent to the total composition of the octahedral layer. Point 1 represents the West Chester, Pennsylvania, vermiculite. Point 2 represents Batavite, and Point 3 is from a calculation on the guidebook analysis, sample 1. Points 4 through 9 are from calculations based on the data in Table 8. Point 4 represents the large crystals (ground to 400 mesh) analysed by x-ray fluorescence and points 5 through 9 are for the 16-32, 4-8, 1-2, and 1/10-1/4 micron fractions where all iron is considered as Fe^{+3}. Titanium is not included here, nor is provision made for the differences in the total number of ions in the octahedral layer. The change in composition from the coarser size fraction through to the finer material is toward a nontronitic chemical composition.

Cation Exchange Capacity

Theoretical cation exchange capacities were calculated for all particle sizes of the size-fractioned material. These are presented in Figure 21 as two curves. Curve A shows the calculations from Table 8, rows numbered 1, in which all iron is considered as Fe^{+3}. Curve B is from data in the same table, but from rows numbered 2 where all iron is considered as Fe^{+2}.

The cation exchange capacities of the 16-32, 4-8, 1-2, 1/2-1, 1/4-1/2, 1/10-1/4 micron samples were measured by the sodium hydroxide continuous titration technique. Figure 21, Curve C shows the data that were obtained from this series of measurements. No claim is made as to the completeness of the exchange reaction in any sample. It is known from x-ray diffraction and DTA analyses that the exchange was only about one-third effected in the 16-32 micron material and about one-half completed in the 4-8 micron fraction. It is thought that the cation exchange capacity did approach completeness in the finer fractions.

Whether or not the cation exchange capacity data represent total exchange, they are of significant value. The variation in cation exchange shows a trend from high values to low values with decreasing particle size which agrees with the trend predicted from the calculated structures. This provides independent evidence supporting the calculations as good approximations of actual structural formulae.

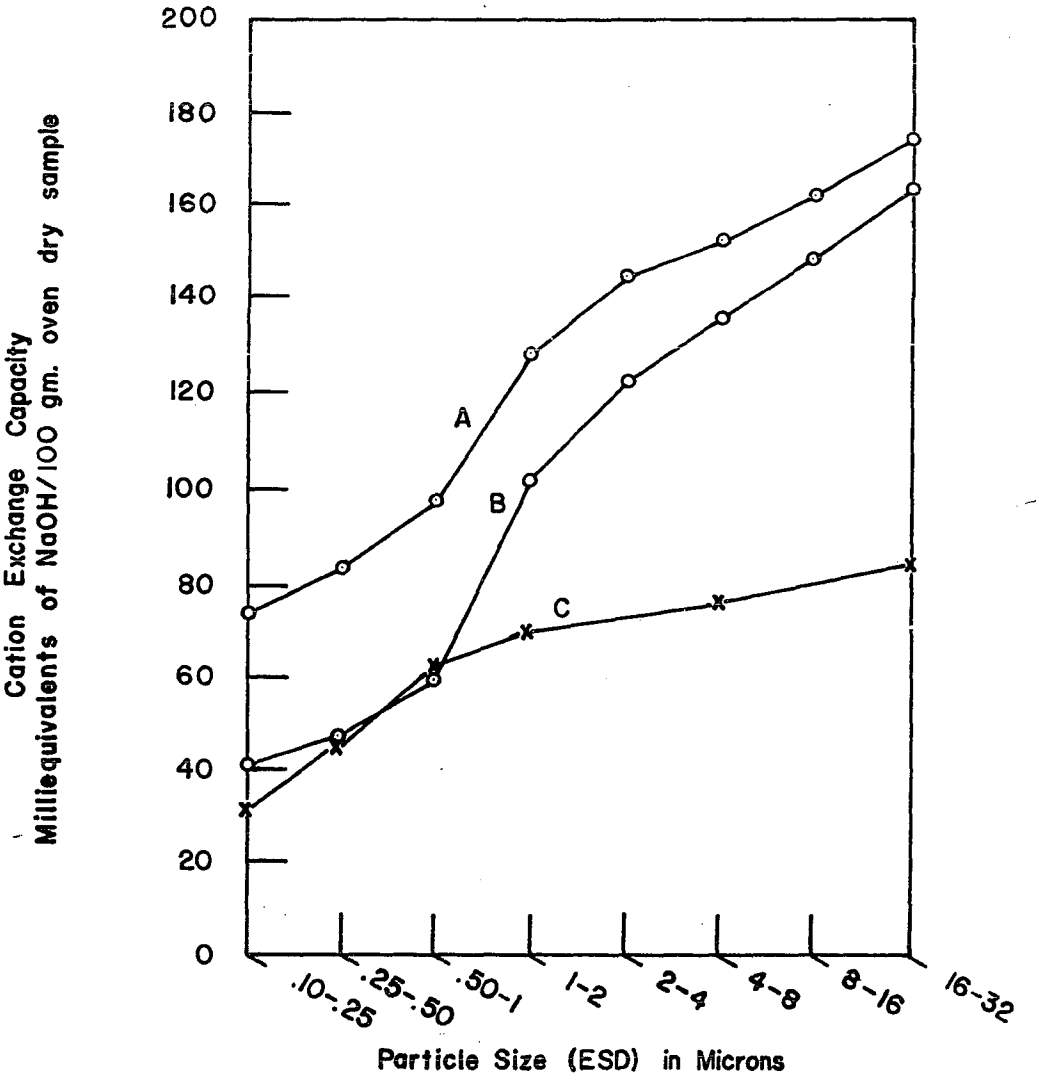

Figure 21. Calculated and measured cation exchange capacities of particle size fractions of Llano vermiculite.

Curve A: CEC calculated, iron considered as Fe^{+3}.
Curve B: CEC calculated, iron considered as Fe^{+2}.
Curve C: CEC measured.

Dioctahedral Nature of the Finer Fraction

The structure of the size-fractioned vermiculite is undoubtedly different in the finer particle sizes as observed in the x-ray diffraction powder data, and from the structural formulae which are supported by the cation exchange capacity and DTA data. If the x-ray data for ethylene glycol expanded samples are considered, the partial stability of the 14.5 Å peak must be explained. Assuming that the non-expandability is due to the stronger bonding forces between charges that are close to the interlayer cation as opposed to the weaker bond strength due to octahedral sites, the expandable lattice may be attributed to a more dioctahedral type of structure (in this case) as opposed to a trioctahedral type of lattice.

It has been shown that the 1/10-1/4 micron material experienced an eighty percent decrease in the intensity of the 14.5 Å peak with solvation. Assuming eighty percent dioctahedral and twenty percent trioctahedral character of the material, a basis for a separation into two distinct lattice configurations is provided. As a composition for the trioctahedral portion, the structural formula for the large crystals as determined from the x-ray fluorescence chemical analysis was assumed. This was justified by small differences between this analysis and that for the 16-32 micron fraction and the total non-expandability of the large crystals. A

structural formula for the large crystals may be written as:

$$(Mg_{2.43}Fe_{0.30}Ti_{0.06})(Si_{3.13}Al_{0.87})O_{10}(OH)_2 \quad \begin{matrix} 0.44\ Mg \\ 0.01\ Ca \\ 0.01\ K \end{matrix}$$

which is taken as the estimated trioctahedral counterpart. Twenty percent of this structural formula was back calculated to gram-atomic ratios and subtracted from the gram-atomic ratios of the 1/10-1/4 micron chemical analysis. The remaining chemical constituents were then converted to half unit-cell ratios by the Marshall method. Considering an ideal dioctahedral structure, that is two ions in the octahedral layer on a half unit-cell basis, the structural formula of the dioctahedral counterpart was found to be:

$$(Fe_{1.00}Al_{0.63}Mg_{0.36}Ti_{0.01})(Si_{3.83}Al_{0.17})O_{10}(OH)_2 \quad \begin{matrix} 0.25\ Mg \\ 0.01\ Ca \\ 0.01\ K \end{matrix}$$

with all iron considered as Fe^{+3}. The cation exchange capacity in this case is somewhat higher than calculated before and does not fit well with the measured value. A more generalized formula could be written as:

$$(Fe_{1.00}Al_{0.63}Mg_{0.36+x}Ti_{0.01})(Si_{3.83}Al_{0.17})O_{10}(OH)_2 \quad \begin{matrix} 0.25\ Mg-x \\ 0.01\ Ca \\ 0.01\ K \end{matrix}$$

thus allowing for slight deviations from an ideally dioctahedral structure. The charge deficiency on the tetrahedral layer is -0.17. The octahedral charge deficiency is somewhat undetermined, but from the generalized formula, may be stated as:

$$(-0.35 + 2x) \qquad 5$$

where x is the additional number of Mg^{+2} ions attributed to the octahedral layer due to deviations from the ideal two ion population. By the same reasoning, the interlayer cation charge may be written as:

$$(+0.53 - 2x) \qquad 6$$

where x has the same significance as above.

Interpretations

X-ray diffraction data provide evidence that the smaller size fractions (less than one micron ESD) of the vermiculite regolith from the Carl Moss Ranch in Llano, Texas, are not true vermiculites. The b-axis parameter of the coarser fractions, calculated from the d-spacings of the (060) peaks, ranges from 9.21 Å to 9.24 Å attesting to the trioctahedral nature of these materials. In the less than one micron samples the (02ℓ), (11ℓ) edge appears at 19.7 degrees two-theta (4.50 Å). An approximate b-axis parameter based on these data is 9.00 Å which is to be expected for dioctahedral micas.

The structural formulae calculated from chemical analyses indicate a more dioctahedral composition for the smaller sized particles. Independent data support these as reasonably good approximations of the actual average structural formulae. Differential thermal analyses show that the interlayer magnesium content is higher in the coarser fraction and decreases with particle size. Although calculated and measured values for the cation exchange capacities are not in

close agreement, they do show the same variation with particle size. The measured CEC decreases with particle size at the same relative rate as values predicted from the calculated structural formulae. Disagreements in CEC values may be primarily the result of fundamental assumptions made for the purpose of standardizing the structural formula calculations. If more magnesium were placed in the octahedral layer, the predicted cation exchange capacities would be somewhat lower. Good CEC data were not obtainable for the larger particles because of the difficulty in approaching a total exchange condition. This is primarily due to incomplete conversions of the coarser-grained vermiculite to the hydrogen form. This could be accomplished if a more rigorous acid treatment were employed. However, this could result in a partial removal of lattice elements as well as interlayer cations and further complicate the interpretation of total cation exchange capacity information.

The heterogeneity of the vermiculite regolith may be predominantly due to a mechanical mixture of distinct phases, each crystallite being fairly homogeneous and crystallite compositions being quite different, but varying within the ranges of two or more distinct modal types. For simplicity's sake, the system may be considered as discrete particles of two end members with the trioctahedral crystallites occupying a coarser particle size distribution and the dioctahedral crystallites concentrated in the smaller size class. If

this is the case, the data may simply be an expression of the higher degree of stability of dioctahedral with respect to trioctahedral micas in a weathering environment.

An alternative is that the heterogeneity of this material is one of mixed domains within individual crystals. In this case it might be reasoned that one phase (dioctahedral type) is an alteration product of the other (trioctahedral type) phase. A "reaction-rim" of fairly constant thickness may exist around an essentially unaltered core. This "reaction-rim" would become increasingly more significant volumetrically as the size of the affected particle was decreased. At some lower size limit, the depth of alteration would result in a completely altered phase. That is, the crystallite would be fairly homogeneous and of a composition similar or identical to the "reaction-rim" of the larger crystallites.

Arguments supporting both alternatives may be equally justified by interpretations of the data presented in this study. The difficulty lies in the fact that the properties observed, measured, and calculated in all cases are average properties of the mixture of two or more phases. Final conclusions become even more difficult to draw if the system is considered as more than a simple two-phase mixture. However, the systematic variation in the chemical composition with particle size suggests that a direct correlation may be made using these parameters. It is probably a justified assumption that the smaller grained material is indeed an alteration

product of the coarser-grained material. If these points are granted, then the choice between the two alternatives stated above is relegated to one of academic interest. The following discussion attempts to present the mechanism or process by which the trioctahedral type of vermiculite may well be expected to alter to a dioctahedral phase similar in composition and properties to that of the fine-grained material.

Weaver (1958) pointed to the inadvisability, or at least the problems, involved in classifying clay minerals on the basis of secondary properties such as swelling. As pointed out by Jonas (1960) these properties are a function of the chemical and physical properties of a particular crystal. If these are in turn a function of particle size, then care should be taken in the assignment of mineral names that would subdivide into separate mineral groups or species, substances that are basically the same. Using principles of crystal chemistry, Jonas described the possiblity of differences in chemical composition that might occur at the boundaries of mineral grains. Referring to the work of Pauling (1948) and data provided by Fyfe (1951), Jonas suggested that the differences in the bond character (percent ionic), as estimated from electronegativity differences of various cations with respect to oxygen, would lead to some interesting reactions at the grain surfaces in an aqueous environment. Under such conditions those cations, in equivalent structural positions, having a higher degree of ionic bond character could be pre-

ferentially dissolved and removed from the lattice. The more commonly occurring cations in clay and mica structures may be arranged in order of decreasing percent of ionic bond character, Mg> Al> Fe^{+2} > Si. Iron as Fe^{+3} and silicon are, more or less equivalent. In the tetrahedral layer, then it might be expected that aluminum ions could be preferentially removed with respect to silicon. At exposed octahedral sites a depletion of magnesium could occur with respect to iron and aluminum ions. Iron would be expected to be preferentially retained in equivalent positions with respect to aluminum.

On this basis, Jonas proposed that such differences in chemical composition at the grain boundaries are negligible when dealing with large macroscopic crystals. As the particle diminished, however, these non-uniform compositional features might affect the overall properties of the substance. Some of the differences between montmorillonite and muscovite may be attributed to such a phenomenon. These would be the lower tetrahedral Al/Si ratio and the lower average surface charge density of the montmorillonites. Jonas (1960), therefore, proposed a model for montmorillonite consisting of an interior with a mica composition and a different composition at the edge.

This same approach can be followed to explain the differences between the structure, chemical composition and properties of the larger and smaller particles of the vermiculite regolith. Preferential solution of cations from equiva-

lent lattice positions by hydrothermal and/or weathering activity could adequately account for observed differences. The Al/Si ratio was shown to systematically decrease with particle size (Fig. 18). Selective removal of magnesium and an increase in the iron and aluminum content is also consistent with this argument. The total effect is one in which the material is altered from a trioctahedral to a more dioctahedral type of structure.

A secondary effect is a relocation of part of the charge deficiency in the octahedral layer. The total surface charge is also decreased and this affects the cation exchange capacity and the low-temperature characteristics of the DTA pattern. The low surface charge density and the transferral of part of the lattice charge sites to the octahedral layer, thus creating a weaker lattice to interlayer cation bond, probably accounts for the more expandable nature of the smaller particles with ethylene glycol treatment.

SWELLING PROPERTIES OF MONTMORILLONITE AND VERMICULITE

Selection of Materials

The three samples selected for this study were chosen so that the site of lattice charge deficiencies of each mineral would be significantly different from the other two. The 1/10-1/2 micron fraction of Plum bentonite montmorillonite has been sufficiently described as a three-layer clay mineral in which the lattice charge deficiencies are predominantly (perhaps totally) limited to octahedral layer substitution. Two samples were selected from the various size-fractions of the vermiculite regolith from Llano, Texas. The 4-8 microns sample was choses to represent a three-layer mica-type mineral in which the lattice charge deficiencies are predominantly (perhaps totally) due to aluminum for silicon substitution in the tetrahedral layers. The 1/10-1/4 micron fraction of the vermiculite regolith represents an intermediate type between the montmorillonite and coarse-grained vermiculite (4-8 microns) in that the charge deficiency is located in both the tetrahedral and octahedral layers, although it is difficult to state the exact distribution. If the samples are arranged in order of the decreasing contribution of the tetrahedral

layer charge deficiency to the total surface charge density in each sample, the order is: Vermiculite (4-8μ) > Vermiculite (1/10-1/4μ) > Montmorillonite (1/10-1/2μ). It is important at this stage to recall the fact that the total surface charge density or cation exchange capacities do not bear the same relationship in these samples. Arranging the same samples on the basis of interlayer cation content or total surface charge from highest to lowest result in: Vermiculite (4-8μ) > Montmorillonite (1/10-1/2μ) > Vermiculite (1/10-1/4μ).

Preparation of Cation Exchanged Samples

Three grams of the 1/10-1/2 micron fraction of the Plum bentonite montmorillonite were converted to the hydrogen ion form with hydrogen resin. This material was then split into seven equal portions and each was washed with a 0.1N chloride salt solution of either lithium, sodium, potassium, magnesium, calcium, strontium, or barium. Samples of the 1/10-1/4 micron and 4-8 microns fractions of the Llano vermiculite regolith were similarly treated. After converting to the hydrogen form these samples were split into four equal portions and washed with 0.1N chloride salt solutions of sodium, potassium, magnesium, and calcium.

The chloride salt washing process was repeated with five hundred milliliters of solution. After adding the solution, the sample was dispersed with the autosonic generator. The material was allowed to stand undisturbed for twelve hours in

which time all samples completely settled from suspension by flocculation. The clear liquid was decanted and another five hundred milliliters of the appropriate salt solution was added. This process was repeated for a total of ten washings.

Excess salt solution was removed after ten washing by flushing the samples with distilled water. This treatment was repeated until the samples showned no flocculation during a twelve hour period. The exchanged samples were then centrifuged, dryed at 60° C, ground to less than eighty mesh powders and stored in glass vials.

Differential Thermal Analysis

Dried powders of the cation exchanged montmorillonite and vermiculite samples were humidified for eight hours at about fifty percent relative humidity and subjected to differential thermal analyses. All thermograms were run with the same Robert L. Stone DTA unit (Model 13M) using an inconel sample holder. The dynamic gas was nitrogen and the unit was calibrated at 1.0 with a microvolt setting of 80. The heating rate was programmed for 10° C per minute.

Figure 22 contains the DTA curves for the untreated and cation exchanged 1/10-1/2 micron fraction of montmorillonite. It is evident that the interlayer cation composition has a direct influence on the shape and position of the low temperature de-watering endotherms. There is also an observable difference in the high temperature exotherms of samples saturated

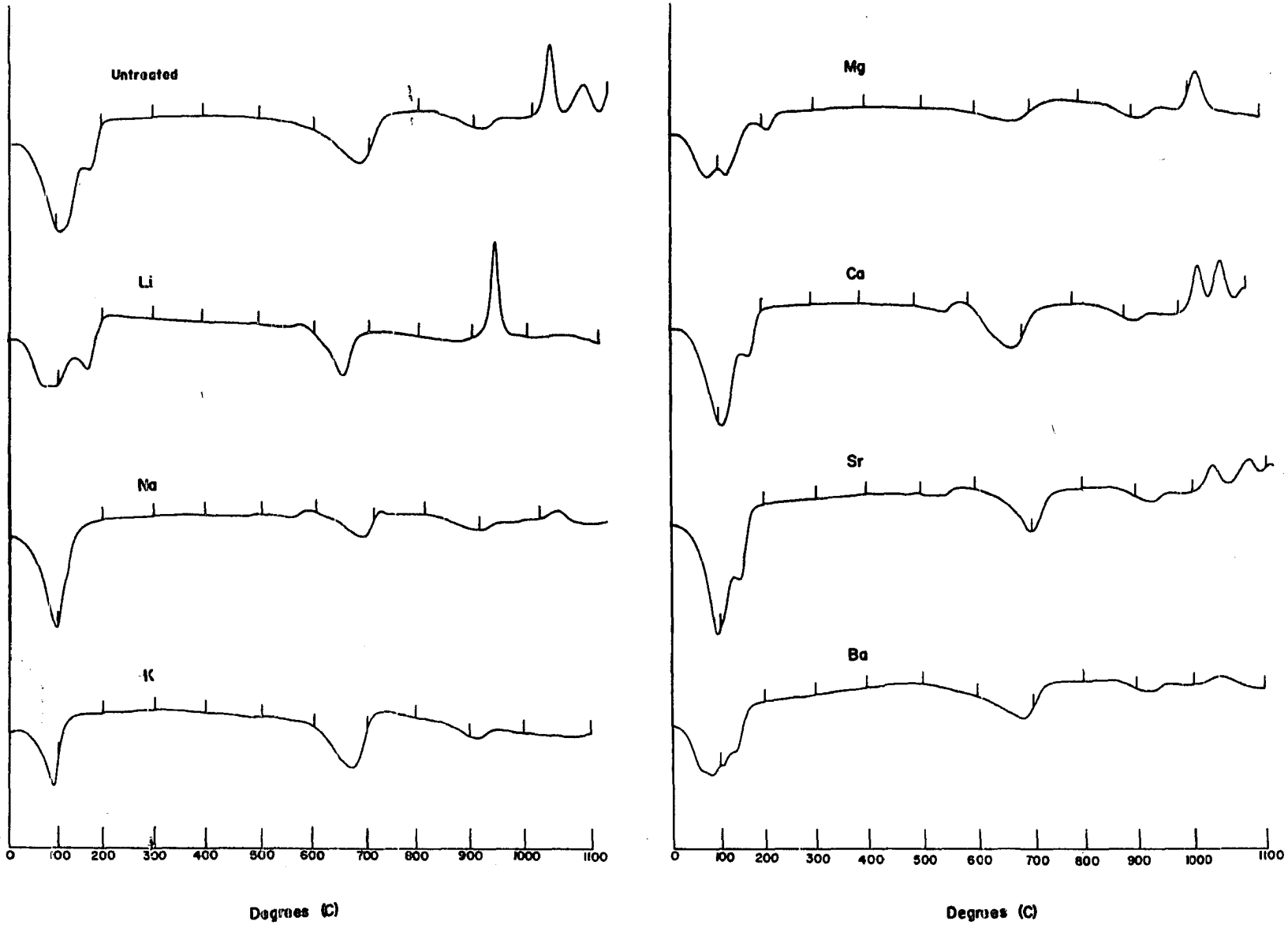

Figure 22. Differential thermal analysis patterns of cation exchanged Plum bentonite montmorillonite (1/10-1/2 micron ESD).

with different cations. The mid-range endothermic reactions at 600-700° C are only slightly modified.

The high temperature phases formed on firing of each of these samples were not considered essential to this study. The shape and position of the low temperature de-watering endotherms are considered of primary importance, however. The temperature at which total dehydration has occurred within the experimental system is reflected in the return of the endothermic curve to the base-line. This is a direct function of the retention of the particular substance for interlayer water. The shape of the endothermic loop is an expression of the dehydration mechanism in each case. The samples saturated with divalent cations are characterized by having more than one node or hump on the low temperature endotherm. The magnesium saturated sample has two nodes of about equal intensity at slightly less and slightly greater than 100° C. A smaller third node is observed at about 210° C. The endotherms for the strontium and calcium saturated samples are nearly identical. These show two partially resolved peaks at 100-200° C. The lower temperature node is more intense than the higher temperature part. Both endotherms of the calcium saturated sample occur at a slightly higher temperature range than those observed for the Sr-montmorillonite sample. The barium saturated sample exhibits four poorly resolved nodes on a broad endotherm that is displaced toward a lower temperature than observed for any of the other divalent cation satu-

rated samples. The lithium saturated sample displays an endothermic doublet similar to the divalent cation exchanged samples. In this thermogram a broad hump reaches maximum intensity at less than 100° C, whereas, a sharper well-resolved node is observed at about 170° C. The sodium and potassium saturated samples have single de-watering endotherms, but with sodium this occurs at a slightly higher temperature (100° C) than observed in the potassium saturated sample (about 90° C). The thermogram for the untreated and calcium exchanged samples are similar as should be expected on the basis of the chemical analyses obtained for this material.

Thermograms of the 4-8 microns and the 1/10-1/4 micron fraction of vermiculite are shown in Figure 23. The untreated and magnesium saturated samples have low temperature de-watering endotherms similar to those observed for the magnesium exchanged montmorillonite sample. The calcium saturated samples again display an endothermic doublet similar to the magnesium samples, but displaced toward a lower temperature. The sodium saturated 4-8 microns sample displays a doublet, but the low temperature shoulder may reflect an incomplete cation exchange. The endotherm for the potassium exchanged 4-8 microns vermiculite is small and indicates little water lost during the de-hydration process. The endotherms for the sodium and potassium exchanged 1/10-1/4 micron vermiculite samples are similar to, although somewhat broader than the montmorillonite analogues.

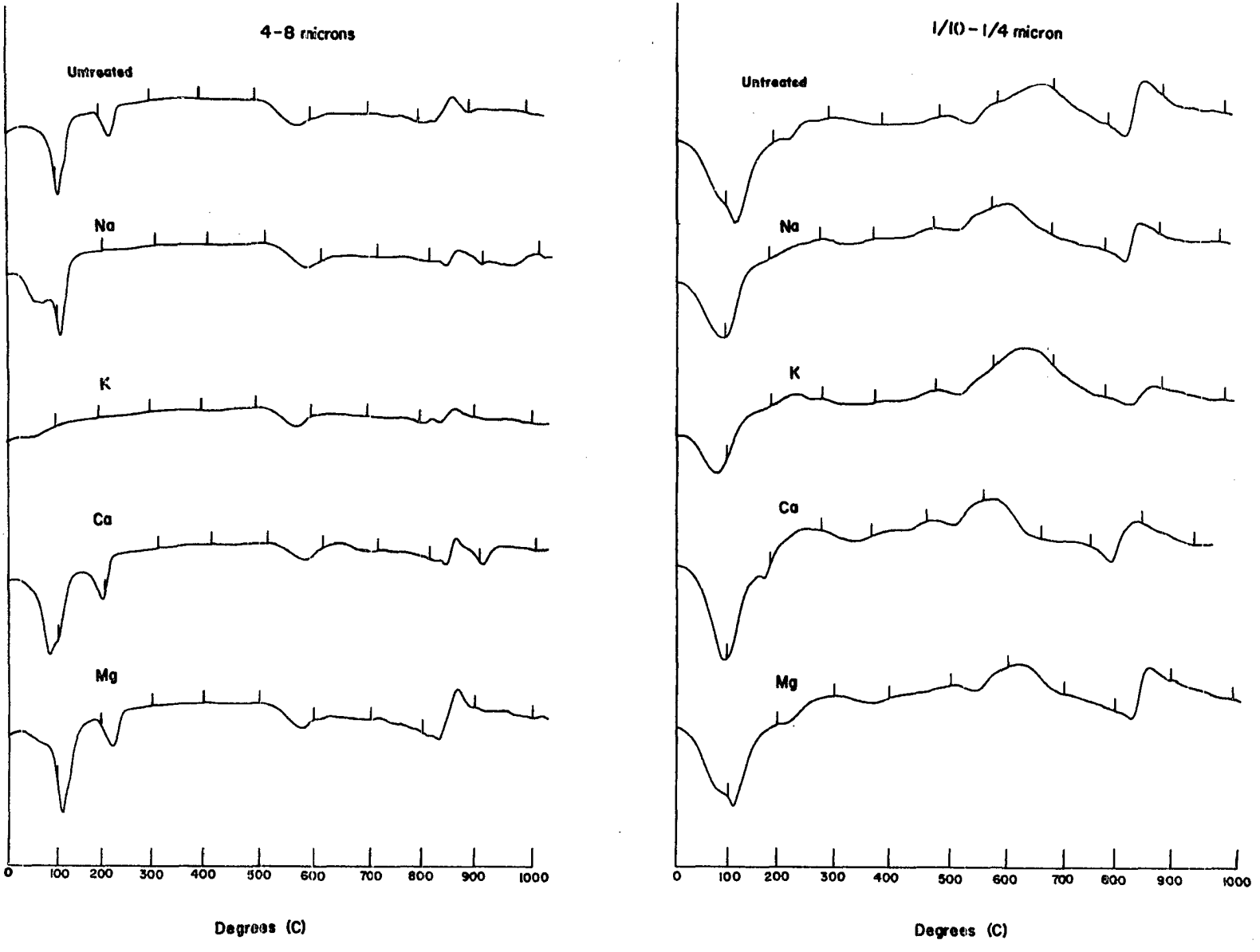

Figure 23. Differential thermal analysis patterns of cation exchanged Llano vermiculite samples.

Controlled Humidity Diffractometer

A small plastic chamber with thin polyethylene plastic windows was designed and fitted over the sample holder of the Siemens x-ray diffractometer. Drying conditions were provided by pumping air through magnesium perchlorate dessicant. Relative humidities of 15, 31, and 88 percent at 24.5° C were also generated and the air flow was directed into the chamber so that it struck the center of the sample mount.

The powdered samples of cation exchanged montmorillonite and vermiculite were prepared as (00ℓ) orientations by sedimenting the dispersed materials on glass slides and drying at 60° C. Each slide was placed in the diffractometer chamber and successively submitted to dry air treatment and 15, 31, and 88 percent relative humidity environments. A minimum of eight hours was allowed for the attainment of equilibrium conditions in each case. A diffractometer scan at 1 degree two-theta per minute was made from two to forty-eight degrees two-theta, after which the scan was repeated over the first principle peak to insure that no change had occurred during the time of measurement.

Zero relative humidity was not achieved with the dry air environment. The relative humidity in this case was reproducible, however, and was certainly less than fifteen percent. The other reported values of relative humidity are thought to be fairly accurate and the deviations were probably less than $\pm$ 2 percent. The main objective of this phase of the investi-

gation was to submit the cation exchanged montmorillonite and vermiculite to the same wide range of reproducible relative humidity conditions and observe the differences in relative amounts and rates of interlayer water absorption as a function of the expansion or increase in the (001) d-spacings.

Tables 10, 11, and 12 list the equilibrium d-spacings for the (00ℓ) oriented samples of cation exchanged montmorillonite and vermiculite samples subjected to different conditions of relative humidity. The first principal peaks of the 4-8 microns vermiculite sample is reported as (001) although technically they are the (002) diffraction peaks. This was done in order to maintain a notation consistent with the other two samples. In many cases the d-spacings of subsequent orders are not precisely converted to (001) d-spacings by integer multiplication. This is due to non-homogeneous hydration between successive stacks of three-layer structural units. In general, however, an increase in total water uptake results in an increase in the (001) d-spacing. The difficulties caused by mixed-layering of structural units with various amounts of interlayer water absorption contribute only to the problem of interpretation of the hydration mechanism.

Figure 24, A and B, shows graphically the equilibrium (001) d-spacings versus relative humidity for the various cation saturated montmorillonite samples. Figure 24-A contains curves for the monovalent cation exchanged samples and Figure 24-B is a similar plot for samples containing divalent

TABLE 10

CONSTANT HUMIDITY X-RAY DATA FOR THE CATION EXCHANGED 1/10-1/2 MICRON (ESD) PLUM BENTONITE MONTMORILLONITE

Interlayer Cation		Relative Humidities in percent (at 25° C) Dry d(Å)	15 d(Å)	31 d(Å)	88 d(Å)
Ba	(001)	10.78	12.28	16.4	16.83
	(002)	5.13	-	-	-
	(003)	3.31	-	5.34	5.37
	(004)	-	3.18	-	-
	(005)	-	-	3.20	3.23
Sr	(001)	11.95	12.63	15.78	16.22
	(002)	5.91	6.19	-	-
	(003)	3.08	-	5.28	5.34
	(004)		3.13	-	-
	(005)	-	-	3.14	3.16
Ca	(001)	12.2	13.28	15.64	16.1
	(002)	5.87	6.56	-	-
	(003)	-	-	5.22	5.31
	(004)	-	3.29	-	-
	(005)	-	-	3.12	3.15
Mg	(001)	13.0	14.14	16.08	16.39
	(002)	6.15	-	-	-
	(003)	-	4.87	5.31	5.40
	(004)	-	3.51	-	-
	(005)	-	-	3.18	3.21
K	(001)	10.5	12.11	12.28	12.32
	(002)	5.05	-	-	-
	(003)	3.35	-	-	-
	(004)	-	3.24	3.24	3.23
Na	(001)	10.04	12.63	15.64	16.4
	(002)	4.90	-	-	-
	(003)	3.23	-	5.22	5.28
	(004)	-	3.16	-	-
	(005)	-	-	3.12	3.13
Li	(001)	12.11	12.54	15.73	16.1
	(002)	5.99	6.15	-	-
	(003)	-	-	5.31	5.34
	(004)	3.03	3.12	-	-
	(005)	-	-	3.12	3.19

TABLE 11

CONSTANT HUMIDITY X-RAY DATA FOR THE CATION EXCHANGED 1/10-1/4 MICRON (ESD) VERMICULITE

Interlayer Cation		Relative Humidities in percent (at 25° C) Dry d(Å)	15 d(Å)	31 d(Å)	88 d(Å)
K	(001)	10.65	12.11	12.3	12.4
	(002)	-	-	-	-
	(003)	3.43		-	-
	(004)	-	3.43	3.10	3.11
Na	(001)	10.4	13.02	14.62	14.62
	(002)	-	-	7.38	7.38
	(003)	3.38	-	4.80	4.90
	(004)	-	-	3.58	3.60
Ca	(001)	11.86	13.39	15.01	15.01
	(002)	-	-	7.44	7.44
	(003)	-	-	4.98	4.98
	(004)	2.93	-	-	-
	(005)	-	-	3.00	3.00
Mg	(001)	11.50	14.20	14.21	14.53
	(002)	-	7.31	7.25	7.25
	(003)	-	4.80	4.82	4.81
	(004)	2.88	3.59	3.60	3.60
	(005)	-	2.87	2.89	2.89

TABLE 12

CONSTANT HUMIDITY X-RAY DATA FOR THE CATION EXCHANGED 4-8 MICRON (ESD) VERMICULITE

Interlayer Cation		Relative Humidities in percent (at 25° C) Dry d(Å)	15 d(Å)	31 d(Å)	88 d(Å)
K	(001)	10.33	10.40	10.46	10.46
	(002)	4.93	4.93	4.93	4.93
	(003)	3.39	3.39	3.39	3.39
	(004)	2.53	2.53	2.53	2.53
	(005)	2.02	2.02	2.02	2.02
Na	(001)	10.04	12.20	14.77	14.80
	(002)	4.87	-	7.38	7.44
	(003)	3.39	-	4.96	4.96
	(004)	-	2.98	3.72	3.72
	(005)	1.96	-	2.99	2.99
	(006)	-	2.00	-	-
Ca	(001)	11.79	12.37	15.11	15.21
	(002)	5.91	-	7.50	7.56
	(003)	-	-	5.04	5.04
	(004)	2.94	3.00	3.77	3.77
	(005)	-	-	3.01	3.02
Mg	(001)	11.55	14.53	14.53	14.54
	(002)	5.79	7.31	7.31	7.25
	(003)	3.83	4.80	4.81	4.82
	(004)	2.88	3.60	3.60	3.63
	(005)	-	2.88	2.87	2.90

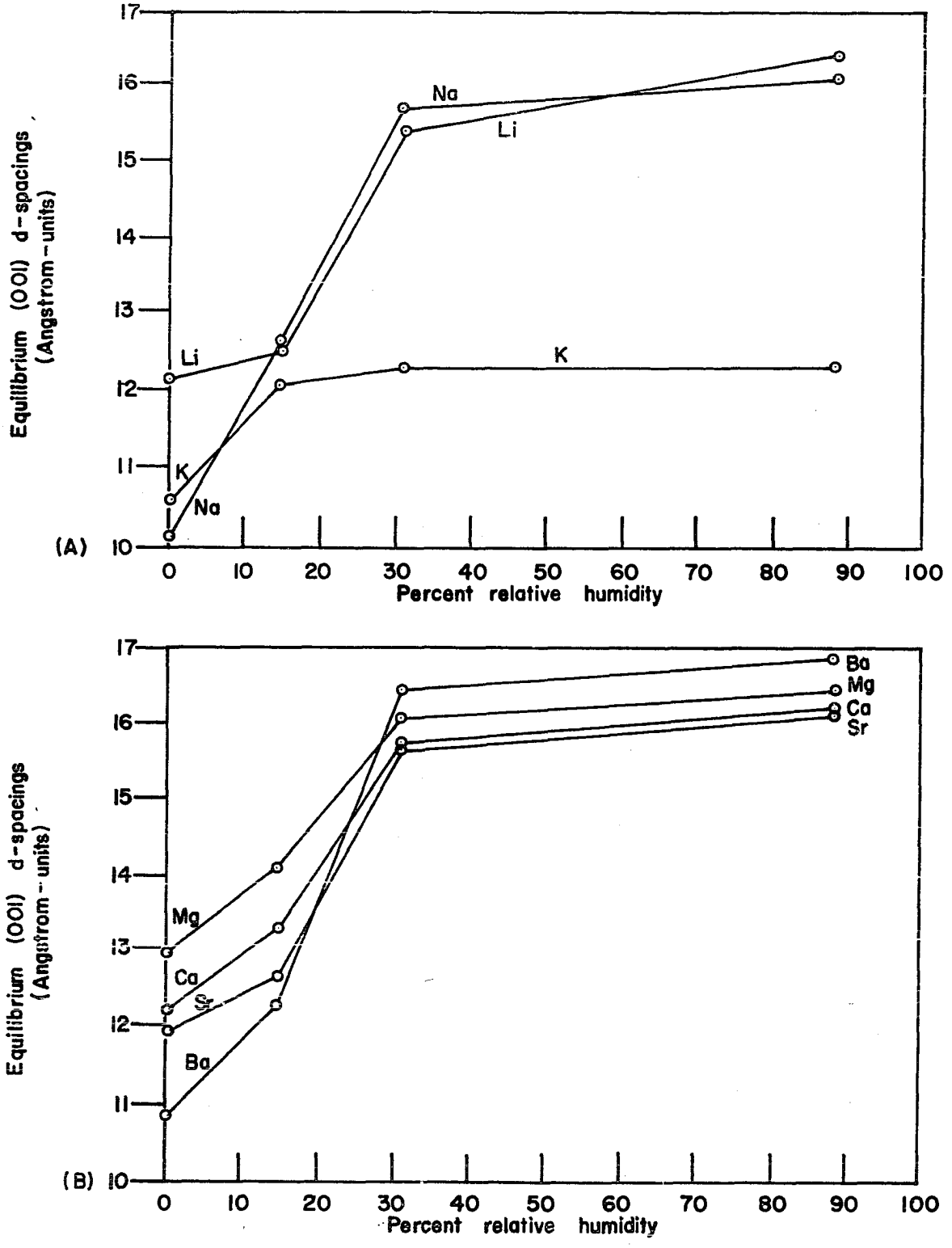

Figure 24. Equilibrium (001) d-spacings of cation exchanged .10-.50 micron Plum bentonite montmorillonite. (A) Equilibrium d-spacings for monovalent-cation exchanged samples. (B) Equilibrium d-spacings for divalent-cation exchanged samples.

interlayer cations. Figures 25 and 26 contain data for the 4-8 microns and 1/10-1/4 micron vermiculite samples.

The relative effect of interlayer cations on the water absorption capacity of expandable three-layer clay minerals may be observed from Figures 24, 25, and 26. The 10-11 Å (001) d-spacings of potassium, sodium, and barium saturated samples indicate an almost totally de-watered state. Other samples containing interlayer magnesium, calcium, strontium, and lithium have somewhat higher (001) d-spacings reflecting a stronger cation to water-molecule bond. Differences in the equilibrium (001) d-spacings at 15 percent relative humidity also reflect differences in the hydration states or degrees of interlayer water absorption. Differences in the "completely" expanded states at 31 and 88 percent relative humidities are thought to be secondary (except for potassium) because at this level the size of the interlayer cation becomes significant and may account for most of the seemingly anomalous differences.

In order to compare the expandable properties of the montmorillonite and vermiculite samples, data from Figures 24, 25, and 26 are replotted in Figure 27. This illustration contains the equilibrium (001) d-spacings for the magnesium and potassium exchanged samples. These particular data were chosen because they represent the extremes of swelling behavior for each of the three substances included in this study.

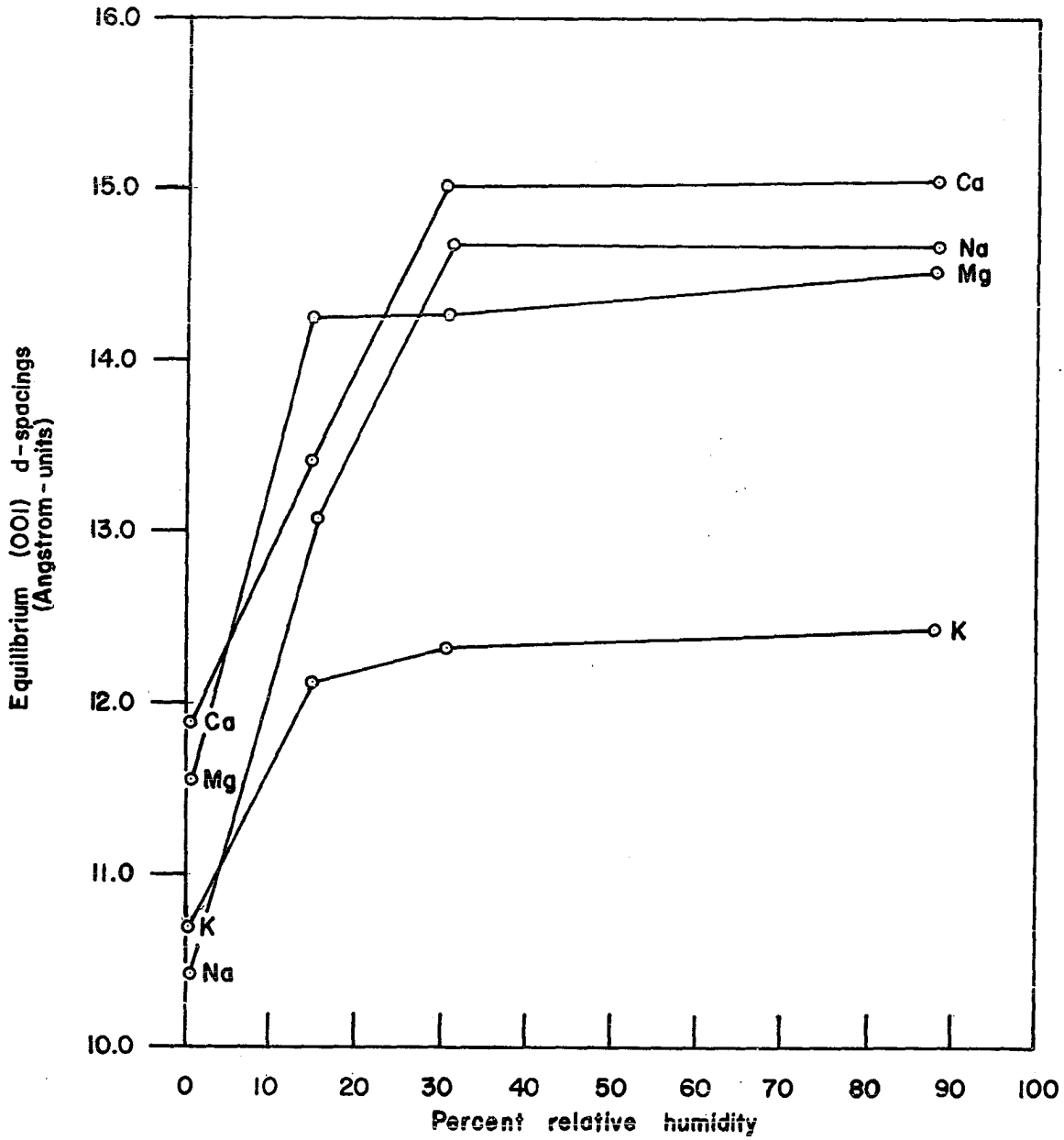

Figure 25. Equilibrium (001) d-spacings for cation exchanged .10-.25 micron Llano vermiculite.

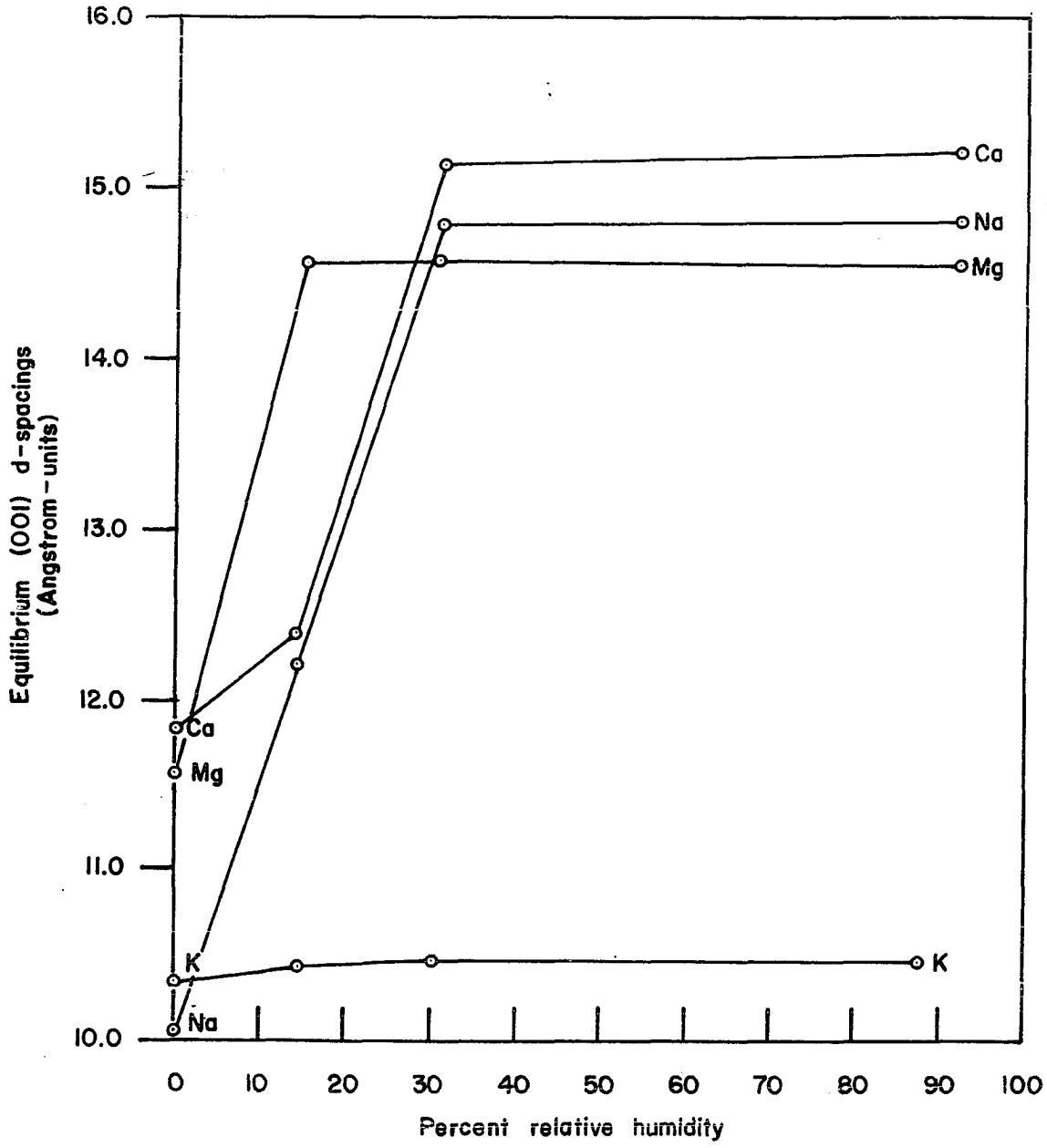

Figure 26. Equilibrium (001) d-spacings for cation exchanged 4-8 micron Llano vermiculite.

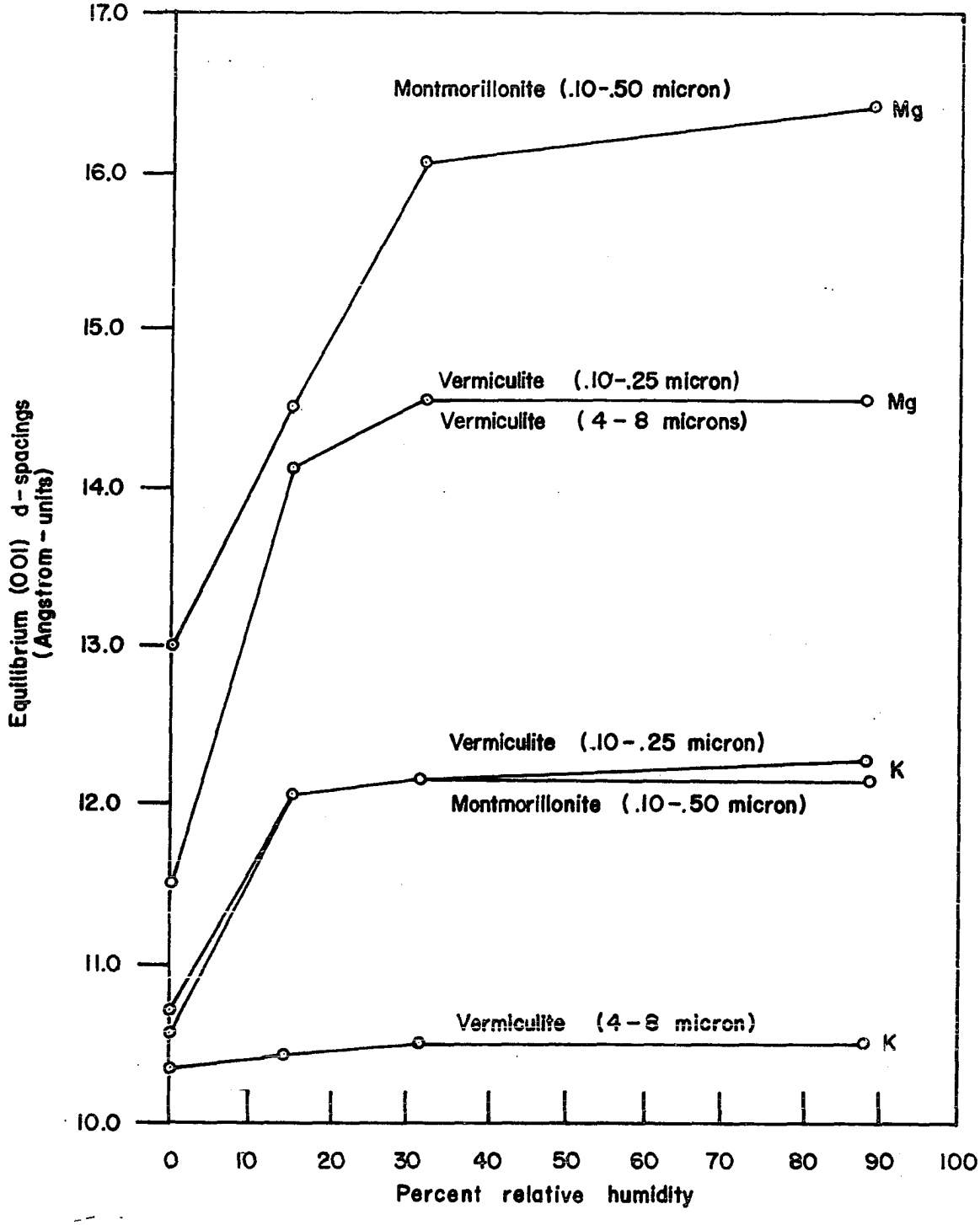

Figure 27. Equilibrium (001) d-spacings for Mg- and K-exchanged .10-.50 micron Plum bentonite montmorillonite, .10-.25 micron Llano vermiculite, and 4-8 microns Llano vermiculite.

The 4-8 microns K-vermiculite sample retained a 10.4 Å collapsed d-spacing over the entire range of relative humidities up to 88 percent. The potassium saturated 1/10-1/2 micron montmorillonite and 1/10-1/4 micron vermiculite samples responded similarly and expanded from dry 10.5 Å and 10.48 Å states to 12.32 Å and 12.4 Å states at 88 percent relative humidity respectively. The magnesium interlayered vermiculites expanded identically from partially collapsed 11.5 Å states to about 14.5 Å at 88 percent relative humidity. Under dry air conditions the magnesium exchanged montmorillonite collapsed to only 13 Å revealing its higher retentive capacity for interlayer water. At 88 percent relative humidity the (001) d-spacing of the montmorillonite expanded to 16.39 Å.

Interpretations

The constant humidity x-ray diffraction data support the concept of cation hydration complex formation. A complete sequence of all possible hydration states was not observed for any one particular sample. This was probably due to the lack of more closely spaced intervals of controlled relative humidity. Non-integral multiples of (00ℓ) d-spacings in some cases also indicate that hydration does not occur uniformly between the layers of all the crystallites. However, Walker's (1956) 11.5 Å state was reproduced. A single mono-molecular water state of about 12.4 Å and the octahedrally coordinated states of 14.5 Å were also observed. The 15 Å states may be interpreted as two mono-molecular water layers or as cubic

coordination states of water molecules with respect to the interlayer cation. The appearance of 16-17 Å states at high relative humidity values may be attributed to the occurrence of mixed two and three mono-molecular water layer states. It may also indicate, particularly in the case of a large cation such as barium, the formation of a twelve-fold coordinated cation-hydration complex. It is not possible on the basis of the limited humidity control under which these data were collected to offer any exacting statement concerning this possibility.

The influence of the interlayer cation composition on the hydration and de-hydration properties of montmorillonite and vermiculite is evident from the DTA and constant humidity x-ray diffractometry data. The endothermic doublets associated with the samples containing the divalent cations of magnesium, barium, and strontium are directly correlated to the occurrence of 14-15 Å equilibrium (001) d-spacings at moderate relative humidities. The first node on the endotherm reflects the shift from an octahedrally coordinated or two mono-molecular water layer configurations to a single mono-molecular water layer state. The second node is due to the removal of the single water layer and a total collapse of the (001) d-spacing to about 10 Å. The single de-watering endotherm of the sodium and potassium saturated samples reflects the (001) d-spacing collapse to 10 Å from a single water-layer 12.4 Å state. The double endotherm of lithium montmo-

rillonite is probably due to a shift from a 12.4 Å single water layer state to the 11.5 Å imperfect octahedrally coordinated configuration (actually a special case of the single water layer state) to a final totally collapsed state. The temperatures at which de-hydration is completed and the relative ease of hydration of the various cation exchanged samples of montmorillonite are in close agreement. From interpretations of the DTA data and the (001) d-spacing data of Figures 24, 25, and 26, an arrangement of the samples from highest to lowest water absorption capacity is:

$$Mg > Ca > Sr > Li > Ba > Na > K.$$

A direct correlation can be made between this property and the radius (r) and the charge (c) of the interlayer cation. The two values may be combined as the ionic potential (c/r) and these data are provided in Table 13. Arranging the interlayer cations on the basis of highest to lowest values of ionic potentials results in:

$$Mg > Ca > Sr > Li > Ba > Na > K.$$

If the interlayer cation composition were the only factor determining the swelling behavior of montmorillonites and vermiculites, then all such minerals possessing the same interlayer cation composition should have the same equilibrium (001) d-spacing under the same conditions of relative humidity. This was not the situation observed in this study as is evidenced by the data plotted in Figure 27. The water absorption capacity of the montmorillonite and vermiculite samples

TABLE 13

ION RADII AND IONIC POTENTIALS FOR SELECTED CATIONS*

Cations	Radius (r)	Ionic Potential (c/r)
	Monovalent Cations	
Li	0.60	1.67
Na	0.95	1.05
K	1.33	0.75
	Divalent Cations	
Mg	0.65	3.08
Ca	0.99	2.02
Sr	1.13	1.77
Ba	1.35	1.48

*Data from Pauling (1940).

are distinctly different. If these are arranged on the basis of relative intensity of expandability over the range of relative humidities considered in this investigation, it may be shown that: Montmorillonite (1/10-1/2μ)>Vermiculite (1/10-1/4μ)> Vermiculite (4-8μ). Because the contributions from the interlayer cations were held constant within the experimental system, some other factor or factors must partially account for the differences in the expanding properties of montmorillonite and vermiculite. The two alternatives that seem possible are the effect of total surface charge density and the site of the charge deficiencies within the lattice. A correlation with respect to total surface charge density is not

possible with the substances included in this investigation. If the three samples are arranged on the basis of increasing surface charge the results are: Vermiculite (1/10-1/4μ)< Montmorillonite (1/10-1/2μ)< Vermiculite (4-8μ). On this basis the 1/10-1/4 micron vermiculite would be expected to expand more readily than the montmorillonite sample under the same interlayer cation and relative humidity conditions. A correlation between the site of lattice charge deficiencies is possible, however. If the three samples are arranged on the basis of distance of separation of the structural charge sites from the interlayer cations, that is, percent octahedral versus tetrahedral charge deficiencies, the results are: Montmorillonite (1/10-1/2μ) > Vermiculite (1/10-1/4μ) > Vermiculite (4-8μ).

SUMMARY AND CONCLUSIONS

Detailed x-ray diffraction, chemical analyses, differential thermal analysis, and cation exchange capacity data were utilized to define the materials used in this study. The Plum bentonite montmorillonite was shown to contain two crystalline phases, alpha-cristobalite and a montmorillonite mineral phase. The non-clay, alpha-cristobalite phase was partially removed by particle size fractionation techniques. The relatively pure 1/10-1/4 micron fraction of the Plum bentonite montmorillonite was shown to have the properties of a Cheto-type montmorillonite. These characteristics are its high octahedrally coordinated magnesium content, high cation exchange capacity, good crystallinity, distinctive DTA characteristics, and the formation of a beta-quartz phase when heated to 1000° C. The structural formula proposed for the Plum bentonite montmorillonite on the basis of these data is:

$$(Al_{1.51}Mg_{0.44}Fe_{0.03}Ti_{0.02})(Si_{3.96}Al_{0.04})O_{10}(OH)_2 \begin{matrix} .19\ Ca \\ .05\ K \end{matrix}$$

Two samples of the Llano vermiculite from the Carl Moss Ranch locality were also rigorously analyzed. Analyses of size-fractioned vermiculite regolith material revealed a progressive variation in the chemistry and structural characteristics of this sample which was associated with particle size.

Larger crystalllites are trioctahedral and are similar to the large macroscopic yellow flakes of vermiculite occurring in veins at the same locality. The less than one micron (ESD) fractions contain considerably more silicon and iron than the more coarsely crystalline material and display distinctly dioctahedral properties. The systematic mineralogical variations which were correlated directly to particle size are interpreted as a reflection of the alteration expected to occur in an aqueous environment. The average structural formula written for the coarse-grained (4-8μ) vermiculite that was selected for more detailed study is:

$$(Mg_{2.09}Fe_{0.47}Al_{0.10}Ti_{0.03})(Si_{3.33}Al_{0.67})O_{10}(OH)_2 \quad \begin{matrix} .28\ Mg \\ .04\ Ca \\ .02\ K \end{matrix}$$

The approximate structural formula for the more dioctahedral 1/10-1/4 micron vermiculite sample may be written as:

$$(Fe_{1.00}Al_{0.63}Mg_{0.36+x}Ti_{0.01})(Si_{3.83}Al_{0.17})O_{10}(OH)_2 \quad \begin{matrix} .25\ Mg\text{-}x \\ .01\ Ca \\ .01\ K \end{matrix}$$

The influence of the interlayer cations on the swelling properties of clay minerals was anticipated. This factor was reduced to a constant by saturating portions of the 1/10-1/2 micron montmorillonite, 1/10-1/4 micron vermiculite and 4-8 microns vermiculite with the same interlayer cations. Samples of montmorillonite were exchanged with lithium, sodium, potassium, magnesium, calcium, strontium, and barium. The vermiculite samples were each separately exchanged with sodium, potassium, magnesium, and calcium. From DTA and controlled

humidity x-ray diffractometry data it was shown that the interlayer cation chemistry does contribute to the absorption capacity of the montmorillonite and vermiculite. An arrangement of the various cation saturated montmorillonite samples from highest to lowest degrees of expandability over a wide range of relative humidities is precisely the same as a listing of the cations on the basis of highest to lowest ionic potential (ionic charge/ionic radius). This series may be written as:

$$Mg > Ca > Sr > Li > Ba > Na > K.$$

X-ray and DTA data for cation exchanged samples of montmorillonite and vermiculite strongly support the concept of cation hydration complex formations as the prevalent expanding mechanism. The two mono-molecular water layer hydration states of 11.5 Å and 12.4 Å were observed. The double mono-molecular water layer states of 14 Å and 15 Å were also reproduced. The 14 Å state is due to the octahedral coordination of water molecules around the interlayer cations, whereas, a cubic coordination state is suggested to account for the 15 Å (001) d-spacings observed at moderate relative humidities. A formation of twelve-fold coordinated complexes at 88 percent relative humidity is a possible explanation for the 16 Å to 17 Å (001) d-spacings, particularly in the case of the barium exchanged sample.

Magnesium and potassium saturated samples exhibited extremely different expanding properties. The constant humidity

x-ray diffraction data for the Mg- and K-saturated samples of montmorillonite and vermiculite were compared. Interpretations of these data lead to the conclusion that the 1/10-1/2 micron montmorillonite exhibited more intense swelling properties or a higher capacity for the absorption of interlayer water than either of the vermiculite samples. The 1/10-1/4 micron vermiculite sample displayed a higher sensitivity to increased relative humidity environments that the 4-8 microns vermiculite sample. A correlation could not be made between the swelling behavior of these three samples and their respective surface charge densitites. However, a direct correlation was made between the swelling properties and the difference in location of lattice charge deficiencies within the montmorillonite and vermiculite lattices. The montmorillonite was observed to have a greater affinity for interlayer water and this may be attributed to the weaker cation to lattice bond arising from predominantly octahedral layer charge deficiencies. The 4-8 microns vermiculite contains predominantly tetrahedral charge deficiency sites which result in a stronger interlayer cation to lattice bond. This property accounts for the more difficultly expandable nature of this substance. The 1/10-1/4 micron vermiculite exhibited swelling properties intermediate between the montmorillonite sample and the 4-8 microns vermiculite. The lattice charge deficiency sites in the fine-grained vermiculite sample were shown to be distributed between the tetrahedral and octahedral layers.

This study has not eliminated the possibility that the total surface charge density of three-layer clay minerals plays an important role in determining the swelling properties of these minerals. This investigation does indicate that the site of the lattice charge deficiency and, therefore, the strength of the interlayer cation to lattice bond also plays an important role in determining whether or not the lattice will be an expanding type.

REFERENCES

Barnes, V. E., and Clabaugh, S. E., 1961, Vermiculite deposits near Llano, Texas: Texas University, Guidebook 3, p. 45-53.

Barshad, I., 1948, Vermiculite and its relation to biotite as revealed by base-exchange reactions, x-ray analyses, differential thermal curves, and water content: American Mineralogist, v. 33, p. 655-678.

_____, 1949, The nature of lattice expansion and its relation to hydration in montmorillonite and vermiculite: American Mineralogist, v. 34, p. 675-684.

_____, 1950, The effect of interlayer cations on the expansion of the mica type crystal lattice: American Mineralogist, v. 35, p. 225-238.

_____, 1955, Absorption and swelling properties of clay-water system: Clays and Clay Technology, California Div. of Mines, Bull. 169, p. 70-77.

Bradley, W. F., Grim, R. E., and Clark, G. L., 1937, A study of the behavior of montmorillonite upon wetting: Z. Kristallog., v. 97, p. 216-222.

Bragg, W. L., 1937, Atomic structure of minerals: Cornell University Press, Ithaca, New York.

Clabaugh, S. E., and Barnes, V. E., 1959, Vermiculite in central Texas: Texas University, Rep. of Invest. 40, 32 p.

Damour, A. A., and Salvetat, _____, 1847, Hydroxilicate d'alumine trouve a montmorillon (Vienne): Ann. Chim. (Phys), (III), v. 21, p. 376-383.

Edelman, C. H., and Favejee, J. C. L., 1940, On the crystal structure of montmorillonite and halloysite: Z. Kristallog., v. 102, p. 417-431.

Folk, R. L., Hayes, M. O., and Brown, T. E., 1961, Tertiary bentonite of central Texas: Texas University, Guidebook 3, p. 5-7.

Foster, M. C., 1960, Interpretation of the composition of trioctahedral micas: U. S. Geol. Survey Prof. Paper 354-B, p. 11-49.

Fyfe, W. S., 1951, Isomorphism and bond type: American Mineralogist, v. 36, p. 538-542.

Grim, R. E., 1953, Clay Mineralogy: McGraw-Hill Book Co., Inc., New York, 384 p.

_____, and Kulbicki, G., 1961, Montmorillonite: High temperature reactions and classification: American Mineralogist, v. 46, p. 1329-1369.

Gruner, J. W., 1934, The structure of vermiculites and their collapse by dehydration: American Mineralogist, v. 19, p. 557-575.

Hendricks, S. B., 1942, Lattice structure of clay minerals and some properties of clays: Jour. Geology, v. 50, p. 276-290.

_____, and Jefferson, M. E., 1938, Structures of kaolin and talc-pyrophyllite hydrates and their bearing on water sorption of the clays: American Mineralogist, v. 23, p. 863-875.

_____, Nelson, R. A., and Alexander, L. T., 1940, Hydration mechanism of clay mineral montmorillonite saturated with various cations: Am. Chem. Soc. Jour., v. 62, p. 1457-1464.

Hofmann, U., et al., 1956, Intracrystalline swelling, cation exchange, and anion exchange of minerals of the montmorillonite group and of kaolin: Clays and Clay Minerals, v. 4, p. 273-287.

_____, and Bilke, W., 1936, Uber die innerkristalline quellung und das Basenaustch-vermogen des Montmorillonits: Kolloidzshr., v. 77, p. 239-251.

_____, Endell, K., and Wilm, D., 1933, Struktur und Quellung von Montmorillonit: Z. Dristallog., v. 86, p. 340-348.

Johns, W. D., and Jonas, E. C., 1954, Some observations on the relation between isomorphism and properties of clays, Jour. Geology, v. 62, p. 163-171.

Jonas, E. C., 1960, Mineralogy of the micaceous clay minerals: Proceedings of the InternationalCommittee for the Study of Clays, Copenhagen, p. 1-16.

_____, 1963, Ion exchange at edge and interlayer in montmorillonites differing in size: Science, v. 140, p. 75-76.

_____, and Roberson, H. E., 1960, Particle size as a factor influencing expansion of the three-layer clay minerals: American Mineralogist, v. 45, p. 828-838.

_____, and Thomas, G. L., 1960, Hydration properties of potassium deficient clay micas: Clays and Clay Minerals, v. 8, p. 183-192.

Kerr, P. F., et al., 1951, Reference clay minerals: American Petroleum Institute Research Project No 49, Columbia University.

MacEwan, D. M. C., 1955, Interlamellar sorption of clay minerals: Clays and Clay Technology, California Div. of Mines, Bull. 169, p. 78-85.

_____, 1961, The montmorillonite minerals, Chap. IV, in x-ray identification and crystal structures of clay minerals: Mineralogical Society, London, 544 p.

MacKenzie, R. C., 1950, Some notes on the hydration of montmorillonite: Clay Min. Bull. 1, p. 115-119.

Maegdefrau, E., and Hofmann, U., 1937, Kristallstructure des Montmorillonits: Z. Kristallog., v. 98, p. 299-323.

Marshall, C. E., 1935, Layer lattices and base exchange clays: Z. Kristallog., v. 91, p. 433-449.

_____, 1949, The colloid chemistry of the silicate minerals: Academic Press, New York, 195 p.

Mathieson, A. McL., and Walker, G. F., 1954, Structure of Mg-vermiculite: American Mineralogist, v. 39, p. 231-255.

McConnell, D., 1950, The crystal chemistry of montmorillonite: American Mineralogist, v. 35, p. 166-172.

Mering, J., 1946, On the hydration of montmorillonite: Trans. Faraday Soc., 42-B, p. 205-219.

Mielenz, R. C., Schieltz, N. C., and King M. E., 1955, Effect of exchangeable cation on x-ray diffraction patterns and thermal behavior of a montmorillonite clay: Clays and Clay Minerals, v. 3, p. 146-173.

Mooney, R. W., Keenan, A. G., and Wood, L. A., 1952, Absorption of water vapor by montmorillonite: Jour. Am. Chem. Soc., v. 74, p. 1367-1374.

Nagelschmidt, G., 1936, On the structure of montmorillonite: Z. Kristallog., v. 93, p. 481-487.

Norrish, K., 1954, Manner of swelling of montmorillonite: Nature, v. 173, p. 256-257.

Paige, S., 1912, Description of the Llano and Burnet quadrangles: U. S. Geol. Surv. Geol. Atlas, Llano-Burnet folio (No. 183), 16 p.

Pauling, L., 1930, The structures of the micas and related minerals: Proc. Nat. Acad. Sci., v. 16, p. 123-129.

_____, 1948, The nature of the chemical bond: Cornell University Press, Ithaca, New York.

Roberson, H. E., 1964, Petrology of tertiary bentonites of Texas: Jour. Sed. Pet., v. 34, p. 401-411.

_____, and Jonas, E. C., 1965, Clay minerals intermediate between illite and montmorillonite: American Mineralogist, v. 50, p. 766-770.

Ross, C. S., 1960, Review of the relationships in the montmorillonite group of clay minerals: Clays and Clay Minerals, v. 7, p. 225-229.

_____, and Hendricks, S. B., 1945, Minerals of the montmorillonite group, their origin and relation to soils and clays: U. S. Geol. Surv. Prof. Paper, 205-B p. 23-79.

Rowland, R. A., Weiss, E. J., and Bradley, W. F., 1956, Dehydration of monoionic montmorillonites: Clays and Clay Minerals, v. 5, p. 85-95.

Sellards, E. H., Adkins, W. S., and Plummer, F. B., 1932, The geology of Texas, v. 1, Stratigraphy: Texas University Bull. 3232, 1007 p.

Walker, G. F., 1950, Trioctahedral minerals in the soil clays of northeast Scotland: Min. Mag., v. 29, p. 72-84.

_____, 1956, The mechanism of dehydration of Mg-vermiculite: Clays and Clay Minerals, v. 4, p. 101-115.

_____, 1961, Vermiculite minerals, Chap. VII, in X-ray identification and crystal structures of clay minerals: Mineralogical Society, London.

Weaver, C. E., 1958a, A discussion on the origin of clay minerals in sedimentary rocks: Clays and Clay Minerals, v. 85, p. 159-173.

_____, 1958b, The effects and geologic significance of potassium "fixation" by expanding clay minerals derived from muscovite, biotite, chlorite, and volcanic material: American Mineralogist, v. 43, p. 839-861.

Weiss, A., and Hofmann, U., 1951, Batavite: Z. Naturforsch., v. 6b., p. 405-409.

White, J. L., 1958, Layer charge and interlayer expansion in a muscovite: Clays and Clay Minerals, v. 5, p. 289-294.